Journal of Computational and Applied Mathematics 236 (2012) 4681–4699

Contents lists available at SciVerse ScienceDirect

Journal of Computational and Applied Mathematics

journal homepage: www.elsevier.com/locate/cam

Linear and bilinear immersed finite elements for planar elasticity interface problems☆

Tao Lin, Xu Zhang*

Department of Mathematics, Virginia Tech, Blacksburg, VA 24061, United States

ARTICLE INFO

Article history:
Received 28 June 2011
Received in revised form 16 March 2012

MSC:
primary 35R05
65N15
65N30
74B05
74S05

Keywords:
Immersed finite element
Discontinuous coefficients
Elasticity interface
Cartesian mesh

ABSTRACT

This article is to discuss the linear (which was proposed in [18,19]) and bilinear immersed finite element (IFE) methods for solving planar elasticity interface problems with structured Cartesian meshes. Basic features of linear and bilinear IFE functions, including the unisolvent property, will be discussed. While both methods have comparable accuracy, the bilinear IFE method requires less time for assembling its algebraic system. Our analysis further indicates that the bilinear IFE functions are guaranteed to be applicable to a larger class of elasticity interface problems than linear IFE functions. Numerical examples are provided to demonstrate that both linear and bilinear IFE spaces have the optimal approximation capability, and that numerical solutions produced by a Galerkin method with these IFE functions for elasticity interface problem also converge optimally in both L^2 and semi-H^1 norms.

1. Introduction

In this paper, we consider the following planar linear elasticity boundary problem with discontinuous Lamé parameters across a smooth material interface Γ:

$$-\operatorname{div}\sigma(\mathbf{u}) = \mathbf{f} \quad \text{in } \Omega, \tag{1.1}$$

$$\mathbf{u} = \mathbf{g} \quad \text{on } \partial\Omega, \tag{1.2}$$

whose solution $\mathbf{u}$ is required to satisfy the following jump conditions across the interface Γ:

$$[\mathbf{u}]_\Gamma = \mathbf{0}, \tag{1.3}$$

$$\left[\sigma(\mathbf{u})\,\mathbf{n}\right]_\Gamma = \mathbf{0}. \tag{1.4}$$

Here we use letters in bold font to denote vector-valued functions and their associated spaces. The notation $\mathbf{u} = (u_1, u_2)^t$ represents the displacement, $\mathbf{f} = (f_1, f_2)^t$ and $\mathbf{g} = (g_1, g_2)^t$ represent the given body force and the given displacement on the boundary $\partial\Omega$, respectively, and $\mathbf{n}$ denotes the normal of the interface Γ. As usual, the strain tensor is denoted by $\epsilon(\mathbf{u}) = \left(\epsilon_{ij}(\mathbf{u})\right)_{1\le i,j\le 2}$ with

$$\epsilon_{ij}(\mathbf{u}) = \frac{1}{2}\left(\frac{\partial u_i}{\partial x_j} + \frac{\partial u_j}{\partial x_i}\right),$$

☆ This work is partially supported by NSF grant DMS-1016313.
* Corresponding author.
E-mail addresses: tlin@math.vt.edu (T. Lin), xuz@vt.edu (X. Zhang).

0377-0427/$ – see front matter © 2012 Elsevier B.V. All rights reserved.
doi:10.1016/j.cam.2012.03.012

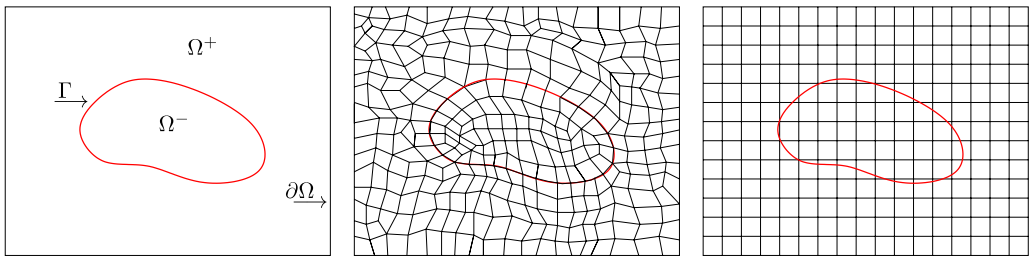

Fig. 1. The plot in the middle shows how elements are placed along an interface in the standard finite element method. The Cartesian mesh on the right are used in the bilinear IFE method, with interface cutting through some rectangles.

and the stress tensor $\sigma(\mathbf{u}) = \left(\sigma_{ij}(\mathbf{u})\right)_{1\le i,j\le 2}$ is defined as

$$\sigma_{ij}(\mathbf{u}) = \lambda\,(\nabla\cdot\mathbf{u})\delta_{ij} + 2\mu\epsilon_{ij}(\mathbf{u}),$$

where λ, μ are Lamé parameters. Without loss of generality, we assume that $\Omega \subset \mathbb{R}^2$ is a rectangular domain (or a union of several rectangular domains) formed with two elastic materials. The interface Γ is a smooth curve that separates these materials into two sub-domains Ω^+, Ω^-, such that $\Omega = \Omega^+ \cup \Omega^- \cup \Gamma$; see the plot on the left in Fig. 1. Hence, the Lamé parameters λ and μ are discontinuous across the interface Γ such that:

$$\lambda = \begin{cases} \lambda^-, & (x,y)^t \in \Omega^-, \\ \lambda^+, & (x,y)^t \in \Omega^+, \end{cases} \qquad \mu = \begin{cases} \mu^-, & (x,y)^t \in \Omega^-, \\ \mu^+, & (x,y)^t \in \Omega^+. \end{cases} \tag{1.5}$$

Many applications in science and engineering require solving the elasticity interface problem (1.1)–(1.4), for instance, problems in the crystalline materials [1], the simulation in the microstructural evolution [2,3], and the atomic interactions [4], to name just a few.

Numerous methods have been developed for solving elasticity problems efficiently and accurately, for instance, finite element methods have been discussed in [5–7] and discontinuous Galerkin methods have been presented in [8–11]. In general, in order to solve an elasticity interface problem, these methods have to use meshes tailored to fit the interface [12,13] ; otherwise, the convergence of numerical solutions produced by these methods cannot be predicted. Such meshes are often called body-fitting as illustrated in the plot in the middle of Fig. 1.

On the other hand, it is usually time consuming to generate a satisfactory body-fitting mesh for an interface problem in which the interface separating the materials is geometrically complicated. Such a difficulty becomes even more severe if the interface evolves in a simulation because a new mesh has to be generated for each of the material configurations to be considered. It is therefore desirable to develop numerical methods that can solve interface problems with a non-body-fitting mesh, such as the Cartesian mesh in the plot on the right in Fig. 1. There have been a few attempts in this direction for the planar elasticity interface problems. Following a Nitsche's idea, the authors in [14,15] have proposed unfitted finite element methods for elasticity interface problems. Using finite difference discretization, the authors in [16,17] have utilized the local coordinate transformation to develop the immersed interface method that allows the material interface to be embedded in the interior of elements.

The recently developed immersed finite element (IFE) methods [17–37] employ an alternative idea to handle interface problems. A main feature of an IFE method is that its mesh can be independent of the interface; hence, if desired, a Cartesian mesh can be used even if the interface geometry is nontrivial. Standard finite element functions are used in non-interface elements, but IFE functions constructed according to the interface jump conditions are employed in interface elements. We note that most of the IFE methods are developed for interface problems involving the popular second order elliptic operator. For elasticity interface problems, the authors in [18,37] present a conforming linear IFE method whose global IFE basis functions have a rather complicated and large support around the interface. A nonconforming linear IFE method on the triangular Cartesian mesh for elasticity interface problem was proposed in [17,19,37] whose authors conclude that this method has at least the first order convergence in a discrete L^∞ norm.

In our article here, we will first recall the linear IFE functions developed in [19] and present a simpler alternative description. Our main focus is to develop a bilinear IFE space based on a rectangular mesh. We note that the bilinear IFE method is more efficient because a Cartesian mesh is simpler than its related Cartesian triangular mesh. Also, our analysis indicates that bilinear IFE functions are guaranteed to be applicable for elasticity interface problems with a larger class of elasticity material configurations than linear IFE functions.

The rest of this paper is organized as follows. In Section 2, we recall the linear IFE functions introduced in [19] and we will provide an alternative formulation that can help our analysis in many situations. In Section 3, we introduce a bilinear IFE space based on a rectangular mesh. In Section 4, we will discuss properties of these IFE spaces including their approximation capability. In Section 5, we will apply these IFE functions in a Galerkin formulation to solve the planar elasticity interface problems. Brief conclusions will be given in Section 6.

2. The linear immersed finite element space

In this section, we first recall the linear IFE functions for the planar elasticity interface problem introduced in [19], and then give a simpler alternative formulation for these IFE functions.

2.1. Linear IFE functions

Let $\mathcal{T}_h = \{T\}$ be a Cartesian triangular mesh of a rectangular domain Ω which is formed by partitioning Ω into uniform rectangles and further cutting each rectangle into two congruent triangles along one of the diagonal line. We call a triangle $T \in \mathcal{T}_h$ an interface triangle if the interface Γ passes through the interior of T; otherwise we call it a non-interface triangle. We will use $\mathcal{T}_h^i$ and $\mathcal{T}_h^n$ to denote the collections of interface triangles and non-interface triangles, respectively. The usual linear finite element functions are used on each $T \in \mathcal{T}_h^n$. For each $T = \Delta A_1A_2A_3 \in \mathcal{T}_h^i$ with vertices

$$A_1 = (x_1, y_1)^t, \qquad A_2 = (x_2, y_2)^t, \qquad A_3 = (x_3, y_3)^t,$$

we assume Γ intersects ∂T at $D = (x_D, y_D)^t$, and $E = (x_E, y_E)^t$ on two different edges of T, and we call them interface points. The line segment $\overline{DE}$, which is used to approximate the actual interface $\Gamma \cap T$, separates T into two polygonal domains T^+ and T^-, among which T^+ is the one containing a vertex in Ω^+. As introduced in [19], piecewise linear polynomials are used to construct linear IFE functions on an interface element T in the following form:

$$\boldsymbol{\Phi}(x, y) = \boldsymbol{\Phi}^s(x, y) = \begin{pmatrix} \phi_1^s(x, y) \\ \phi_2^s(x, y) \end{pmatrix}, \quad \text{if } (x, y)^t \in T^s,\ s = +, -, \tag{2.1}$$

where

$$\phi_j^s(x, y) = a_j^s + b_j^s x + c_j^s y, \quad j = 1, 2,\ s = +, -. \tag{2.2}$$

Note that each linear IFE function described by (2.1) has 12 degrees of freedom (coefficients) $a_j^s, b_j^s, c_j^s, j = 1, 2, s = +, -$; hence, we need 12 restrictions to determine all the coefficients. The nodal values at the vertices of T provide 6 restrictions. The displacement continuity $[\mathbf{u}] = \mathbf{0}$ at interface points D, E provides 4 restrictions. The other 2 restrictions come from the traction continuity $[\sigma(\mathbf{u})\, \mathbf{n}_{\overline{DE}}] = \mathbf{0}$. More details can be found in [19].

2.2. A reduced formulation for linear IFE functions

Here we present an alternative approach to construct linear IFE functions which has a simpler form but is mathematically equivalent to the above definition originally introduced in [19]. We follow the idea used in [23,25] to represent an IFE function in terms of the linear combination of the standard linear finite element nodal basis functions. As usual, we can develop linear IFE functions $\hat{\boldsymbol{\Phi}}(\hat{x}, \hat{y})$ on the reference interface triangle $\hat{T} = \Delta\hat{A}_1\hat{A}_2\hat{A}_3$ whose vertices are:

$$\hat{A}_1 = \begin{pmatrix} 0 \\ 0 \end{pmatrix}, \qquad \hat{A}_2 = \begin{pmatrix} 1 \\ 0 \end{pmatrix}, \qquad \hat{A}_3 = \begin{pmatrix} 0 \\ 1 \end{pmatrix}.$$

Assume an actual element T is the image of the reference element $\hat{T}$ by the following affine mapping:

$$F : \hat{T} \to T, \quad \text{with} \quad X = F(\hat{X}) = M\hat{X} + B, \tag{2.3}$$

where $X = (x, y)^t$ and $\hat{X} = (\hat{x}, \hat{y})^t$. With a proper choice of M and B, we can assume, through this affine mapping, that the pre-images of the interface points $D = (x_D, y_D)^t$ and $E = (x_E, y_E)^t$ are

$$\hat{D} = \begin{pmatrix} 0 \\ \hat{d} \end{pmatrix}, \qquad \hat{E} = \begin{pmatrix} \hat{e} \\ 1 - \hat{e} \end{pmatrix}, \tag{2.4}$$

where $0 < \hat{d},\ \hat{e} \leq 1$. Finally, every IFE function $\boldsymbol{\Phi}(X)$ on the actual element T is defined by an IFE function $\hat{\boldsymbol{\Phi}}(\hat{X})$ on $\hat{T}$ as follows

$$\boldsymbol{\Phi}(X) = \hat{\boldsymbol{\Phi}}(F^{-1}(X)) = \hat{\boldsymbol{\Phi}}(\hat{X}). \tag{2.5}$$

On the reference element $\hat{T}$, we recall the standard scalar linear nodal basis functions: $\hat{\psi}_1 = 1 - \hat{x} - \hat{y}$, $\hat{\psi}_2 = \hat{x}$, $\hat{\psi}_3 = \hat{y}$. We use these scalar functions to form 6 vector nodal basis functions as follows:

$$\hat{\boldsymbol{\Psi}}_i(\hat{x}, \hat{y}) = \begin{pmatrix} \hat{\psi}_i(\hat{x}, \hat{y}) \\ 0 \end{pmatrix}, \quad \text{for } i = 1, 2, 3, \quad \text{and} \quad \hat{\boldsymbol{\Psi}}_i(\hat{x}, \hat{y}) = \begin{pmatrix} 0 \\ \hat{\psi}_{i-3}(\hat{x}, \hat{y}) \end{pmatrix}, \quad \text{for } i = 4, 5, 6. \tag{2.6}$$

The linear vector finite element nodal basis functions on the actual element T corresponding to (2.6) are denoted as $\boldsymbol{\Psi}_{i,T}(x, y),\ 1 \leq i \leq 6$.

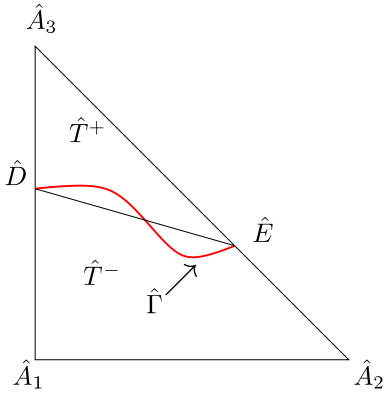

Fig. 2. A reference triangle of interface elements.

Then, for the representative interface configuration in Fig. 2, we can write the vector linear IFE functions in the following form:

$$\hat{\boldsymbol{\Phi}}(\hat{x},\hat{y}) = \hat{\boldsymbol{\Phi}}^s(\hat{x},\hat{y}), \quad \text{if } (\hat{x},\hat{y}) \in \hat{T}^s,\ s = +,-, \tag{2.7}$$

where

$$\hat{\boldsymbol{\Phi}}^-(\hat{x},\hat{y}) = v_1\hat{\boldsymbol{\Psi}}_1(\hat{x},\hat{y}) + v_2\hat{\boldsymbol{\Psi}}_2(\hat{x},\hat{y}) + c_3\hat{\boldsymbol{\Psi}}_3(\hat{x},\hat{y}) + v_4\hat{\boldsymbol{\Psi}}_4(\hat{x},\hat{y}) + v_5\hat{\boldsymbol{\Psi}}_5(\hat{x},\hat{y}) + c_6\hat{\boldsymbol{\Psi}}_6(\hat{x},\hat{y}), \tag{2.8}$$

$$\hat{\boldsymbol{\Phi}}^+(\hat{x},\hat{y}) = c_1\hat{\boldsymbol{\Psi}}_1(\hat{x},\hat{y}) + c_2\hat{\boldsymbol{\Psi}}_2(\hat{x},\hat{y}) + v_3\hat{\boldsymbol{\Psi}}_3(\hat{x},\hat{y}) + c_4\hat{\boldsymbol{\Psi}}_4(\hat{x},\hat{y}) + c_5\hat{\boldsymbol{\Psi}}_5(\hat{x},\hat{y}) + v_6\hat{\boldsymbol{\Psi}}_6(\hat{x},\hat{y}). \tag{2.9}$$

We note that coefficients v_i, $1 \le i \le 6$ are determined by the nodal values of $\hat{\boldsymbol{\Phi}}(\hat{x},\hat{y})$ because we can easily verify that

$$\hat{\boldsymbol{\Phi}}(\hat{A}_1) = \begin{pmatrix} v_1 \\ v_4 \end{pmatrix}, \qquad \hat{\boldsymbol{\Phi}}(\hat{A}_2) = \begin{pmatrix} v_2 \\ v_5 \end{pmatrix}, \qquad \hat{\boldsymbol{\Phi}}(\hat{A}_3) = \begin{pmatrix} v_3 \\ v_6 \end{pmatrix}.$$

The coefficients c_i, $1 \le i \le 6$ are to be determined according to v_i, $1 \le i \le 6$ by imposing the following jump conditions to $\hat{\boldsymbol{\Phi}}$:

$$\hat{\boldsymbol{\Phi}}^+(\hat{D}) = \hat{\boldsymbol{\Phi}}^-(\hat{D}), \qquad \hat{\boldsymbol{\Phi}}^+(\hat{E}) = \hat{\boldsymbol{\Phi}}^-(\hat{E}), \qquad \left(\hat{\sigma}(\hat{\boldsymbol{\Phi}}^+) - \hat{\sigma}(\hat{\boldsymbol{\Phi}}^-)\right)\hat{\mathbf{n}}_{\widehat{\hat{D}\hat{E}}} = \mathbf{0}, \tag{2.10}$$

where $\hat{\sigma}$ is the stress tensor on the reference element and $\hat{\mathbf{n}}_{\widehat{\hat{D}\hat{E}}}$ is the image of $\mathbf{n}_{\overline{DE}}$ through the affine mapping. Specifically, (2.10) leads to the following algebraic system for determining c_i, $1 \le i \le 6$:

$$M_C\mathbf{C} = M_V\mathbf{V}, \quad \mathbf{C} = (c_1, c_2, \ldots, c_6)^t,\ \mathbf{V} = (v_1, v_2, \ldots, v_6)^t, \tag{2.11}$$

where

$$M_C = \begin{pmatrix} 1-\hat{d} & 0 & -\hat{d} & 0 & 0 & 0 \\ 0 & 0 & 0 & 1-\hat{d} & 0 & -\hat{d} \\ 0 & \hat{e} & -1+\hat{e} & 0 & 0 & 0 \\ 0 & 0 & 0 & 0 & \hat{e} & -1+\hat{e} \\ \hat{e}\mu^+ - \hat{r}\omega^+ & \hat{r}\omega^+ & \hat{e}\mu^- & \hat{e}\mu^+ - \hat{r}\lambda^+ & -\hat{e}\mu^+ & -\hat{r}\lambda^- \\ \hat{e}\lambda^+ - \hat{r}\mu^+ & -\hat{e}\lambda^+ & -\hat{r}\mu^- & \hat{e}\omega^+ - \hat{r}\mu^+ & \hat{r}\mu^+ & \hat{e}\omega^- \end{pmatrix}, \tag{2.12}$$

and

$$M_V = \begin{pmatrix} 1-\hat{d} & 0 & -\hat{d} & 0 & 0 & 0 \\ 0 & 0 & 0 & 1-\hat{d} & 0 & -\hat{d} \\ 0 & \hat{e} & -1+\hat{e} & 0 & 0 & 0 \\ 0 & 0 & 0 & 0 & \hat{e} & -1+\hat{e} \\ \hat{e}\mu^- - \hat{r}\omega^- & \hat{r}\omega^- & \hat{e}\mu^+ & \hat{e}\mu^- - \hat{r}\lambda^- & -\hat{e}\mu^- & -\hat{r}\lambda^+ \\ \hat{e}\lambda^- - \hat{r}\mu^- & -\hat{e}\lambda^- & -\hat{r}\mu^+ & \hat{e}\omega^- - \hat{r}\mu^- & \hat{r}\mu^- & \hat{e}\omega^+ \end{pmatrix}, \tag{2.13}$$

with $\omega^s = \lambda^s + 2\mu^s$, $s = +,-$, and $\hat{r} = 1 - \hat{d} - \hat{e}$. Using $\mathbf{V} = \mathbf{V}_i = \mathbf{e}_i \in \mathbb{R}^6$, $1 \le i \le 6$ as the usual i-th basis vector, we can solve (2.11) for $\mathbf{C}_i$ and use them in (2.7) to obtain the i-th IFE nodal basis function $\hat{\boldsymbol{\Phi}}_i(\hat{x},\hat{y})$, $1 \le i \le 6$. Furthermore, using the affine mapping between the reference element $\hat{T}$ and the actual element T, we obtain the i-th linear IFE nodal basis function on T as follows:

$$\boldsymbol{\Phi}_{i,T}(X) = \hat{\boldsymbol{\Phi}}_i(F^{-1}(X)) = \hat{\boldsymbol{\Phi}}_i(\hat{X}), \quad 1 \le i \le 6.$$

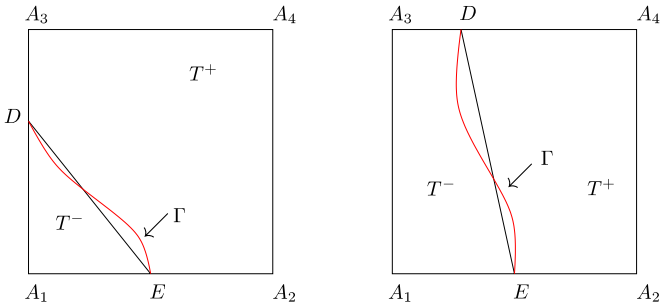

Fig. 3. Interface rectangles: Type I on the left and Type II on the right.

Finally, on each element $T \in \mathcal{T}_h$, we define the local linear IFE space $\mathbf{S}_h(T)$ as

$$\mathbf{S}_h(T) = \begin{cases} \text{span}\{\boldsymbol{\Phi}_{i,T},\ 1 \le i \le 6\}, & \text{if } T \text{ is an interface triangle,} \\ \text{span}\{\boldsymbol{\Psi}_{i,T},\ 1 \le i \le 6\}, & \text{otherwise.} \end{cases} \tag{2.14}$$

We call (2.7) a reduced formulation for linear IFE nodal basis functions because it has 6 undetermined coefficients instead of 12 in the original formulation (2.1).

3. The bilinear immersed finite element spaces

In this section, we first introduce the bilinear IFE functions defined on a Cartesian (rectangular) mesh. Again, a reduced formulation will be employed. Corresponding bilinear IFE spaces for planar elasticity interface problems will be then formed accordingly.

3.1. Bilinear IFE functions

It is more natural and often desirable to use a Cartesian mesh on a rectangular domain (or a union of multiple rectangular domains). Correspondingly, bilinear polynomials will be used to form basis functions on each rectangular element. Let $\mathcal{T}_h = \{T\}$ be a Cartesian mesh of Ω. The interface rectangles are those whose interiors are cut through by the interface Γ, and non-interface rectangles are the rest. Without loss of generality, we assume that elements in a rectangular mesh have the following properties when the mesh size h is small enough:

(H_1): The interface Γ will not intersect an edge of any rectangular element at more than two points unless this edge is part of Γ.

(H_2): If Γ intersects the boundary of a rectangular element at two points, then these two points must be on different edges of this element.

We note that these assumptions are introduced in [26] for discussing scalar elliptic interface problems. As before, we use $\mathcal{T}_h^i$ and $\mathcal{T}_h^n$ to denote the sets of interface rectangles and non-interface rectangles, respectively. Our major concern is to construct basis functions for interface elements. For each $T \in \mathcal{T}_h^i$, we assume $T = \square A_1A_2A_3A_4$ with vertices:

$$A_1 = (x_1, y_1)^t, \qquad A_2 = (x_2, y_2)^t, \qquad A_3 = (x_3, y_3)^t, \qquad A_4 = (x_4, x_4)^t.$$

Assume the interface Γ intersects ∂T at $D = (x_D, y_D)^t$, and $E = (x_E, y_E)^t$. We use the line segment $\overline{DE}$ to approximate the actual interface $\Gamma \cap T$. Note that $\overline{DE}$ separates T into two subelements T^+ and T^-, among which T^+ is the one containing a vertex in Ω^+. Also note that there are two types of rectangular interface element. A Type I interface rectangle is that for which the interface intersects two of its adjacent edges; a Type II interface rectangle is that for which the interface intersects two of its opposite edges. See Fig. 3 for an illustration.

On an interface element T, we define bilinear IFE functions as vector piecewise bilinear polynomials $\boldsymbol{\Phi}$ defined according to the sub-elements T^+ and T^- as follows:

$$\boldsymbol{\Phi}(x, y) = \boldsymbol{\Phi}^s(x, y) = \begin{pmatrix} \phi_1^s(x, y) \\ \phi_2^s(x, y) \end{pmatrix}, \quad \text{if } (x, y)^t \in T^s,\ s = +, -, \tag{3.1}$$

where

$$\phi_j^s(x, y) = a_j^s + b_j^s x + c_j^s y + d_j^s xy, \quad j = 1, 2,\ s = +, -. \tag{3.2}$$

Note that there are 16 undetermined coefficients for each vector-valued bilinear IFE function $\boldsymbol{\Phi}$. The nodal values provide 8 restrictions. We then incorporate interface jump conditions (1.3) and (1.4) to obtain another 8 restrictions in the following

way. Since $\mathbf{\Phi}(x, y)$ is piecewise bilinear, the stress defined through $\mathbf{\Phi}(x, y)$ will not be a constant tensor, therefore we weakly impose the traction continuity in the following integration form:

$$\int_{\overline{DE}} \left(\sigma(\mathbf{\Phi}^+) - \sigma(\mathbf{\Phi}^-)\right) \mathbf{n}_{\overline{DE}}\, \mathrm{d}s = \mathbf{0},$$

which generates 2 restrictions. We can impose another 6 restrictions by requiring the continuity of $\mathbf{\Phi}$ at three points D, E, and $\frac{D+E}{2}$. However, following the idea used for scalar bilinear IFE functions [25,26], we replace the continuity of $\mathbf{\Phi}$ at the midpoint $\frac{D+E}{2}$ by

$$\frac{\partial^2 \mathbf{\Phi}^+}{\partial x \partial y} = \frac{\partial^2 \mathbf{\Phi}^-}{\partial x \partial y}. \tag{3.3}$$

In summary, each bilinear IFE function $\mathbf{\Phi}(x, y)$ defined by (3.1) will be determined by the following conditions:

- the nodal values restrictions:

$$\mathbf{\Phi}(A_j) = \mathbf{V}_j, \quad j = 1, 2, 3, 4,$$

- the displacement interface continuity restrictions:

$$\mathbf{\Phi}^+(D) = \mathbf{\Phi}^-(D), \qquad \mathbf{\Phi}^+(E) = \mathbf{\Phi}^-(E), \qquad \frac{\partial^2 \mathbf{\Phi}^+}{\partial x \partial y} = \frac{\partial^2 \mathbf{\Phi}^-}{\partial x \partial y},$$

- the weak traction interface continuity restrictions:

$$\int_{\overline{DE}} \left(\sigma(\mathbf{\Phi}^+) - \sigma(\mathbf{\Phi}^-)\right) \mathbf{n}_{\overline{DE}}\, \mathrm{d}s = \mathbf{0}.$$

3.2. A reduced formulation for bilinear IFE functions

We now present a reduced formulation for vector bilinear IFE functions. We first consider local bilinear IFE basis functions $\hat{\mathbf{\Phi}}$ on the reference interface rectangle $\hat{T} = \square \hat{A}_1\hat{A}_2\hat{A}_3\hat{A}_4$ with vertices:

$$\hat{A}_1 = \begin{pmatrix} 0 \\ 0 \end{pmatrix}, \qquad \hat{A}_2 = \begin{pmatrix} 1 \\ 0 \end{pmatrix}, \qquad \hat{A}_3 = \begin{pmatrix} 0 \\ 1 \end{pmatrix}, \qquad \hat{A}_4 = \begin{pmatrix} 1 \\ 1 \end{pmatrix}.$$

We assume that an actual element T is associated with the reference element $\hat{T}$ via an affine mapping in the form of (2.3) such that the pre-images of the interface points $D = (x_D, y_D)^t$ and $E = (x_E, y_E)^t$ are

$$\hat{D} = \begin{pmatrix} 0 \\ \hat{d} \end{pmatrix}, \qquad \hat{E} = \begin{pmatrix} \hat{e} \\ 0 \end{pmatrix}, \tag{3.4}$$

with $0 < \hat{d}, \hat{e} \leq 1$ for Type I reference interface rectangle and

$$\hat{D} = \begin{pmatrix} \hat{d} \\ 1 \end{pmatrix}, \qquad \hat{E} = \begin{pmatrix} \hat{e} \\ 0 \end{pmatrix}, \tag{3.5}$$

for Type II reference interface rectangle with $0 < \hat{d}, \hat{e} < 1$, as illustrated in Fig. 4. IFE functions in the actual element T are defined by

$$\mathbf{\Phi}(X) = \hat{\mathbf{\Phi}}(F^{-1}(X)) = \hat{\mathbf{\Phi}}(\hat{X}).$$

On the reference rectangle $\hat{T}$, we recall the standard scalar bilinear nodal basis:

$$\hat{\psi}_1(X) = 1 - \hat{x} - \hat{y} + \hat{x}\hat{y}, \qquad \hat{\psi}_2(X) = \hat{x} - \hat{x}\hat{y}, \qquad \hat{\psi}_3(X) = \hat{y} - \hat{x}\hat{y}, \qquad \hat{\psi}_4(X) = \hat{x}\hat{y},$$

which are used to form 8 vector-valued nodal basis functions in the following forms:

$$\hat{\mathbf{\Psi}}_i(\hat{x}, \hat{y}) = \begin{pmatrix} \hat{\psi}_i(\hat{x}, \hat{y}) \\ 0 \end{pmatrix}, \quad \text{for } i = 1, 2, 3, 4, \quad \text{and} \quad \hat{\mathbf{\Psi}}_i(\hat{x}, \hat{y}) = \begin{pmatrix} 0 \\ \hat{\psi}_{i-4}(\hat{x}, \hat{y}) \end{pmatrix}, \quad \text{for } i = 5, 6, 7, 8. \tag{3.6}$$

The vector bilinear finite element nodal basis functions on an actual element T corresponding to (3.6) are denoted as $\mathbf{\Psi}_{i,T}(x, y)$, $1 \leq i \leq 8$.

On the reference interface rectangle $\hat{T}$, we write the vector bilinear IFE functions as follows:

$$\hat{\mathbf{\Phi}}(\hat{x}, \hat{y}) = \hat{\mathbf{\Phi}}^s(\hat{x}, \hat{y}), \quad \text{if } (\hat{x}, \hat{y})^t \in \hat{T}^s,\ s = +, -, \tag{3.7}$$

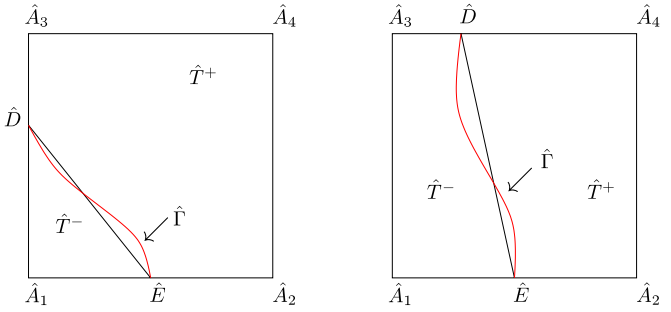

Fig. 4. Reference interface rectangles: Type I on the left and Type II on the right.

where

$$\begin{aligned}\hat{\boldsymbol{\Phi}}^-(\hat{x},\hat{y}) &= v_1\hat{\boldsymbol{\Psi}}_1(\hat{x},\hat{y}) + c_2\hat{\boldsymbol{\Psi}}_2(\hat{x},\hat{y}) + c_3\hat{\boldsymbol{\Psi}}_3(\hat{x},\hat{y}) + c_4\hat{\boldsymbol{\Psi}}_4(\hat{x},\hat{y})\\ &\quad + v_5\hat{\boldsymbol{\Psi}}_5(\hat{x},\hat{y}) + c_6\hat{\boldsymbol{\Psi}}_6(\hat{x},\hat{y}) + c_7\hat{\boldsymbol{\Psi}}_7(\hat{x},\hat{y}) + c_8\hat{\boldsymbol{\Psi}}_8(\hat{x},\hat{y}),\end{aligned} \tag{3.8}$$

$$\begin{aligned}\hat{\boldsymbol{\Phi}}^+(\hat{x},\hat{y}) &= c_1\hat{\boldsymbol{\Psi}}_1(\hat{x},\hat{y}) + v_2\hat{\boldsymbol{\Psi}}_2(\hat{x},\hat{y}) + v_3\hat{\boldsymbol{\Psi}}_3(\hat{x},\hat{y}) + v_4\hat{\boldsymbol{\Psi}}_4(\hat{x},\hat{y})\\ &\quad + c_5\hat{\boldsymbol{\Psi}}_5(\hat{x},\hat{y}) + v_6\hat{\boldsymbol{\Psi}}_6(\hat{x},\hat{y}) + v_7\hat{\boldsymbol{\Psi}}_7(\hat{x},\hat{y}) + v_8\hat{\boldsymbol{\Psi}}_8(\hat{x},\hat{y}),\end{aligned} \tag{3.9}$$

for the Type I reference interface rectangle, and

$$\begin{aligned}\hat{\boldsymbol{\Phi}}^-(\hat{x},\hat{y}) &= v_1\hat{\boldsymbol{\Psi}}_1(\hat{x},\hat{y}) + c_2\hat{\boldsymbol{\Psi}}_2(\hat{x},\hat{y}) + v_3\hat{\boldsymbol{\Psi}}_3(\hat{x},\hat{y}) + c_4\hat{\boldsymbol{\Psi}}_4(\hat{x},\hat{y})\\ &\quad + v_5\hat{\boldsymbol{\Psi}}_5(\hat{x},\hat{y}) + c_6\hat{\boldsymbol{\Psi}}_6(\hat{x},\hat{y}) + v_7\hat{\boldsymbol{\Psi}}_7(\hat{x},\hat{y}) + c_8\hat{\boldsymbol{\Psi}}_8(\hat{x},\hat{y}),\end{aligned} \tag{3.10}$$

$$\begin{aligned}\hat{\boldsymbol{\Phi}}^+(\hat{x},\hat{y}) &= c_1\hat{\boldsymbol{\Psi}}_1(\hat{x},\hat{y}) + v_2\hat{\boldsymbol{\Psi}}_2(\hat{x},\hat{y}) + c_3\hat{\boldsymbol{\Psi}}_3(\hat{x},\hat{y}) + v_4\hat{\boldsymbol{\Psi}}_4(\hat{x},\hat{y})\\ &\quad + c_5\hat{\boldsymbol{\Psi}}_5(\hat{x},\hat{y}) + v_6\hat{\boldsymbol{\Psi}}_6(\hat{x},\hat{y}) + c_7\hat{\boldsymbol{\Psi}}_7(\hat{x},\hat{y}) + v_8\hat{\boldsymbol{\Psi}}_8(\hat{x},\hat{y}),\end{aligned} \tag{3.11}$$

for the Type II reference interface rectangle. Here the coefficients v_i, $i = 1,\ldots,8$ are determined by nodal values of $\hat{\boldsymbol{\Phi}}(\hat{x},\hat{y})$ since we have:

$$\hat{\boldsymbol{\Phi}}(\hat{A}_1) = \begin{pmatrix} v_1 \\ v_5 \end{pmatrix}, \qquad \hat{\boldsymbol{\Phi}}(\hat{A}_2) = \begin{pmatrix} v_2 \\ v_6 \end{pmatrix}, \qquad \hat{\boldsymbol{\Phi}}(\hat{A}_3) = \begin{pmatrix} v_3 \\ v_7 \end{pmatrix}, \qquad \hat{\boldsymbol{\Phi}}(\hat{A}_4) = \begin{pmatrix} v_4 \\ v_8 \end{pmatrix}.$$

The coefficients c_i, $i = 1,\ldots,8$ can be determined according to v_i, $i = 1,\ldots,8$ by imposing the jump conditions to $\hat{\boldsymbol{\Phi}}$:

$$\hat{\boldsymbol{\Phi}}^+(\hat{D}) = \hat{\boldsymbol{\Phi}}^-(\hat{D}), \qquad \hat{\boldsymbol{\Phi}}^+(\hat{E}) = \hat{\boldsymbol{\Phi}}^-(\hat{E}), \qquad \frac{\partial^2\hat{\boldsymbol{\Phi}}^+}{\partial\hat{x}\partial\hat{y}} = \frac{\partial^2\hat{\boldsymbol{\Phi}}^-}{\partial\hat{x}\partial\hat{y}}, \tag{3.12}$$

$$\int_{\widehat{D\hat{E}}} \left(\hat{\sigma}(\hat{\boldsymbol{\Phi}}^+) - \hat{\sigma}(\hat{\boldsymbol{\Phi}}^-)\right)\hat{\mathbf{n}}_{\widehat{D\hat{E}}}\,\mathrm{d}s = \mathbf{0}, \tag{3.13}$$

where $\hat{\sigma}$ is the stress tensor on the reference rectangle, and $\hat{\mathbf{n}}_{\widehat{D\hat{E}}}$ is the image of $\mathbf{n}_{\overline{DE}}$ through the above affine mapping. To be more specific, (3.12) and (3.13) yield the following algebraic systems for unknowns c_i, $i = 1,\ldots,8$:

$$M_C\mathbf{C} = M_V\mathbf{V}, \quad \mathbf{C} = (c_1, c_2, \ldots, c_8)^t, \ \mathbf{V} = (v_1, v_2, \ldots, v_8)^t. \tag{3.14}$$

To simplify the notations, we let $\hat{p} = 2 - \hat{d}$, and $\hat{q} = 2 - \hat{e}$. For Type I reference rectangle, we have

$$M_C = M_C^{\mathrm{I}} = \begin{pmatrix} 1-\hat{d} & 0 & -\hat{d} & 0 & 0 & 0 & 0 & 0 \\ 0 & 0 & 0 & 0 & 1-\hat{d} & 0 & -\hat{d} & 0 \\ 1-\hat{e} & -\hat{e} & 0 & 0 & 0 & 0 & 0 & 0 \\ 0 & 0 & 0 & 0 & 1-\hat{e} & -\hat{e} & 0 & 0 \\ 1 & 1 & 1 & -1 & 0 & 0 & 0 & 0 \\ 0 & 0 & 0 & 0 & 1 & 1 & 1 & -1 \\ m^{\mathrm{I}}_{C71} & m^{\mathrm{I}}_{C72} & m^{\mathrm{I}}_{C73} & m^{\mathrm{I}}_{C74} & m^{\mathrm{I}}_{C75} & m^{\mathrm{I}}_{C76} & m^{\mathrm{I}}_{C77} & m^{\mathrm{I}}_{C78} \\ m^{\mathrm{I}}_{C81} & m^{\mathrm{I}}_{C82} & m^{\mathrm{I}}_{C83} & m^{\mathrm{I}}_{C84} & m^{\mathrm{I}}_{C85} & m^{\mathrm{I}}_{C86} & m^{\mathrm{I}}_{C87} & m^{\mathrm{I}}_{C88} \end{pmatrix}, \tag{3.15}$$

where

$$\begin{aligned} &m^{\mathrm{I}}_{C71} = \hat{d}\hat{p}\omega^+ + \hat{e}\hat{q}\mu^+, \quad m^{\mathrm{I}}_{C72} = \hat{d}\hat{p}\omega^- - \hat{e}^2\mu^-, \quad m^{\mathrm{I}}_{C73} = \hat{e}\hat{q}\mu^- - \hat{d}^2\omega^-, \quad m^{\mathrm{I}}_{C74} = \hat{d}^2\omega^- + \hat{e}^2\mu^-,\\ &m^{\mathrm{I}}_{C75} = \hat{d}\hat{q}\lambda^+ + \hat{e}\hat{p}\mu^+, \quad m^{\mathrm{I}}_{C76} = \hat{e}\hat{p}\mu^- - \hat{d}\hat{e}\lambda^-, \quad m^{\mathrm{I}}_{C77} = \hat{d}\hat{q}\lambda^- - \hat{d}\hat{e}\mu^-, \quad m^{\mathrm{I}}_{C78} = \hat{d}\hat{e}\lambda^- + \hat{d}\hat{e}\mu^-,\\ &m^{\mathrm{I}}_{C81} = \hat{e}\hat{p}\lambda^+ + \hat{d}\hat{q}\mu^+, \quad m^{\mathrm{I}}_{C82} = \hat{e}\hat{p}\lambda^- - \hat{d}\hat{e}\mu^-, \quad m^{\mathrm{I}}_{C83} = \hat{d}\hat{q}\mu^- - \hat{d}\hat{e}\lambda^-, \quad m^{\mathrm{I}}_{C84} = \hat{d}\hat{e}\lambda^- + \hat{d}\hat{e}\mu^-,\\ &m^{\mathrm{I}}_{C85} = \hat{e}\hat{q}\omega^+ + \hat{d}\hat{p}\mu^+, \quad m^{\mathrm{I}}_{C86} = \hat{d}\hat{p}\mu^- - \hat{e}^2\omega^-, \quad m^{\mathrm{I}}_{C87} = \hat{e}\hat{q}\omega^- - \hat{d}^2\mu^-, \quad m^{\mathrm{I}}_{C88} = \hat{e}^2\omega^- + \hat{d}^2\mu^-, \end{aligned}$$

and

$$M_V = M_V^{\mathrm{I}} = \begin{pmatrix} 1-\hat{d} & 0 & -\hat{d} & 0 & 0 & 0 & 0 & 0 \\ 0 & 0 & 0 & 0 & 1-\hat{d} & 0 & -\hat{d} & 0 \\ 1-\hat{e} & -\hat{e} & 0 & 0 & 0 & 0 & 0 & 0 \\ 0 & 0 & 0 & 0 & 1-\hat{e} & -\hat{e} & 0 & 0 \\ 1 & 1 & 1 & -1 & 0 & 0 & 0 & 0 \\ 0 & 0 & 0 & 0 & 1 & 1 & 1 & -1 \\ m_{V71}^{\mathrm{I}} & m_{V72}^{\mathrm{I}} & m_{V73}^{\mathrm{I}} & m_{V74}^{\mathrm{I}} & m_{V75}^{\mathrm{I}} & m_{V76}^{\mathrm{I}} & m_{V77}^{\mathrm{I}} & m_{V78}^{\mathrm{I}} \\ m_{V81}^{\mathrm{I}} & m_{V82}^{\mathrm{I}} & m_{V83}^{\mathrm{I}} & m_{V84}^{\mathrm{I}} & m_{V85}^{\mathrm{I}} & m_{V86}^{\mathrm{I}} & m_{V87}^{\mathrm{I}} & m_{V88}^{\mathrm{I}} \end{pmatrix}, \tag{3.16}$$

where

$$\begin{aligned} &m_{V71}^{\mathrm{I}} = \hat{d}\hat{p}\omega^- + \hat{e}\hat{q}\mu^-, \quad m_{V72}^{\mathrm{I}} = \hat{d}\hat{p}\omega^+ - \hat{e}^2\mu^+, \quad m_{V73}^{\mathrm{I}} = \hat{e}\hat{q}\mu^+ - \hat{d}^2\omega^+, \quad m_{V74}^{\mathrm{I}} = \hat{d}^2\omega^+ + \hat{e}^2\mu^+, \\ &m_{V75}^{\mathrm{I}} = \hat{d}\hat{q}\lambda^- + \hat{e}\hat{p}\mu^-, \quad m_{V76}^{\mathrm{I}} = \hat{e}\hat{p}\mu^+ - \hat{d}\hat{e}\lambda^+, \quad m_{V77}^{\mathrm{I}} = \hat{d}\hat{q}\lambda^+ - \hat{d}\hat{e}\mu^+, \quad m_{V78}^{\mathrm{I}} = \hat{d}\hat{e}\lambda^+ + \hat{d}\hat{e}\mu^+, \\ &m_{V81}^{\mathrm{I}} = \hat{e}\hat{p}\lambda^- + \hat{d}\hat{q}\mu^-, \quad m_{V82}^{\mathrm{I}} = \hat{e}\hat{p}\lambda^+ - \hat{d}\hat{e}\mu^+, \quad m_{V83}^{\mathrm{I}} = \hat{d}\hat{q}\mu^+ - \hat{d}\hat{e}\lambda^+, \quad m_{V84}^{\mathrm{I}} = \hat{d}\hat{e}\lambda^+ + \hat{d}\hat{e}\mu^+, \\ &m_{V85}^{\mathrm{I}} = \hat{e}\hat{q}\omega^- + \hat{d}\hat{p}\mu^-, \quad m_{V86}^{\mathrm{I}} = \hat{d}\hat{p}\mu^+ - \hat{e}^2\omega^+, \quad m_{V87}^{\mathrm{I}} = \hat{e}\hat{q}\omega^+ - \hat{d}^2\mu^+, \quad m_{V88}^{\mathrm{I}} = \hat{e}^2\omega^+ + \hat{d}^2\mu^+. \end{aligned}$$

For Type II reference rectangle, we have

$$M_C = M_C^{\mathrm{II}} = \begin{pmatrix} 0 & 0 & 1-\hat{d} & -\hat{d} & 0 & 0 & 0 & 0 \\ 0 & 0 & 0 & 0 & 0 & 0 & 1-\hat{d} & -\hat{d} \\ 1-\hat{e} & -\hat{e} & 0 & 0 & 0 & 0 & 0 & 0 \\ 0 & 0 & 0 & 0 & 1-\hat{e} & -\hat{e} & 0 & 0 \\ 1 & 1 & -1 & -1 & 0 & 0 & 0 & 0 \\ 0 & 0 & 0 & 0 & 1 & 1 & -1 & -1 \\ m_{C71}^{\mathrm{II}} & m_{C72}^{\mathrm{II}} & m_{C73}^{\mathrm{II}} & m_{C74}^{\mathrm{II}} & m_{C75}^{\mathrm{II}} & m_{C76}^{\mathrm{II}} & m_{C77}^{\mathrm{II}} & m_{C78}^{\mathrm{II}} \\ m_{C81}^{\mathrm{II}} & m_{C82}^{\mathrm{II}} & m_{C83}^{\mathrm{II}} & m_{C84}^{\mathrm{II}} & m_{C85}^{\mathrm{II}} & m_{C86}^{\mathrm{II}} & m_{C87}^{\mathrm{II}} & m_{C88}^{\mathrm{I}} \end{pmatrix}, \tag{3.17}$$

where

$$\begin{aligned} &m_{C71}^{\mathrm{II}} = \omega^+ - (\hat{d}\hat{p} - \hat{e}\hat{q})\mu^+, \quad m_{C81}^{\mathrm{II}} = -(\hat{d} - \hat{e})\lambda^+ + (2 - \hat{d} - \hat{e})\mu^+, \\ &m_{C72}^{\mathrm{II}} = \omega^- + (\hat{d}^2 - \hat{e}^2)\mu^-, \quad m_{C82}^{\mathrm{II}} = -(\hat{d} - \hat{e})\lambda^- - (\hat{d} + \hat{e})\mu^-, \\ &m_{C73}^{\mathrm{II}} = \omega^+ + (\hat{d}\hat{p} - \hat{e}\hat{q})\mu^+, \quad m_{C83}^{\mathrm{II}} = -(\hat{d} - \hat{e})\lambda^+ - (2 - \hat{d} - \hat{e})\mu^+, \\ &m_{C74}^{\mathrm{II}} = \omega^- - (\hat{d}^2 - \hat{e}^2)\mu^-, \quad m_{C84}^{\mathrm{II}} = -(\hat{d} - \hat{e})\lambda^- + (\hat{d} + \hat{e})\mu^-, \\ &m_{C75}^{\mathrm{II}} = (2 - \hat{d} - \hat{e})\lambda^+ - (\hat{d} - \hat{e})\mu^+, \quad m_{C85}^{\mathrm{II}} = -(\hat{d}\hat{p} - \hat{e}\hat{q})\omega^+, \\ &m_{C76}^{\mathrm{II}} = -(\hat{d} + \hat{e})\lambda^- - (\hat{d} - \hat{e})\mu^-, \quad m_{C86}^{\mathrm{II}} = (\hat{d}^2 - \hat{e}^2)\omega^- + \mu^-, \\ &m_{C77}^{\mathrm{II}} = -(2 - \hat{d} - \hat{e})\lambda^+ - (\hat{d} - \hat{e})\mu^+, \quad m_{C87}^{\mathrm{II}} = (\hat{d}\hat{p} - \hat{e}\hat{q})\omega^+, \\ &m_{C78}^{\mathrm{II}} = (\hat{d} + \hat{e})\lambda^- - (\hat{d} - \hat{e})\mu^-, \quad m_{C88}^{\mathrm{II}} = -(\hat{d}^2 - \hat{e}^2)\omega^- + \mu^-, \end{aligned}$$

and

$$M_V = M_V^{\mathrm{II}} = \begin{pmatrix} 0 & 0 & 1-\hat{d} & -\hat{d} & 0 & 0 & 0 & 0 \\ 0 & 0 & 0 & 0 & 0 & 0 & 1-\hat{d} & -\hat{d} \\ 1-\hat{e} & -\hat{e} & 0 & 0 & 0 & 0 & 0 & 0 \\ 0 & 0 & 0 & 0 & 1-\hat{e} & -\hat{e} & 0 & 0 \\ 1 & 1 & -1 & -1 & 0 & 0 & 0 & 0 \\ 0 & 0 & 0 & 0 & 1 & 1 & -1 & -1 \\ m_{V71}^{\mathrm{II}} & m_{V72}^{\mathrm{II}} & m_{V73}^{\mathrm{II}} & m_{V74}^{\mathrm{II}} & m_{V75}^{\mathrm{II}} & m_{V76}^{\mathrm{II}} & m_{V77}^{\mathrm{II}} & m_{V78}^{\mathrm{II}} \\ m_{V81}^{\mathrm{II}} & m_{V82}^{\mathrm{II}} & m_{V83}^{\mathrm{II}} & m_{V84}^{\mathrm{II}} & m_{V85}^{\mathrm{II}} & m_{V86}^{\mathrm{II}} & m_{V87}^{\mathrm{II}} & m_{V88}^{\mathrm{I}} \end{pmatrix}, \tag{3.18}$$

where

$$\begin{aligned} &m_{V71}^{\mathrm{II}} = \omega^- - (\hat{d}\hat{p} - \hat{e}\hat{q})\mu^-, \quad m_{V81}^{\mathrm{II}} = -(\hat{d} - \hat{e})\lambda^- + (2 - \hat{d} - \hat{e})\mu^-, \\ &m_{V72}^{\mathrm{II}} = \omega^+ + (\hat{d}^2 - \hat{e}^2)\mu^+, \quad m_{V82}^{\mathrm{II}} = -(\hat{d} - \hat{e})\lambda^+ - (\hat{d} + \hat{e})\mu^+, \\ &m_{V73}^{\mathrm{II}} = \omega^- + (\hat{d}\hat{p} - \hat{e}\hat{q})\mu^-, \quad m_{V83}^{\mathrm{II}} = -(\hat{d} - \hat{e})\lambda^- - (2 - \hat{d} - \hat{e})\mu^-, \\ &m_{V74}^{\mathrm{II}} = \omega^+ - (\hat{d}^2 - \hat{e}^2)\mu^+, \quad m_{V84}^{\mathrm{II}} = -(\hat{d} - \hat{e})\lambda^+ + (\hat{d} + \hat{e})\mu^+, \\ &m_{V75}^{\mathrm{II}} = (2 - \hat{d} - \hat{e})\lambda^- - (\hat{d} - \hat{e})\mu^-, \quad m_{V85}^{\mathrm{II}} = -(\hat{d}\hat{p} - \hat{e}\hat{q})\omega^-, \end{aligned}$$

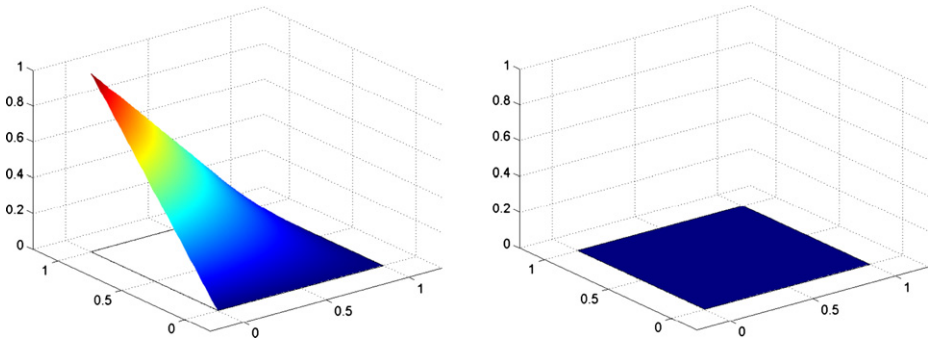

Fig. 5. The standard elasticity bilinear basis function $\hat{\mathbf{\Phi}}_3$: the left plot is for the first component $\hat{\psi}_3$, and the right one is for the second component 0.

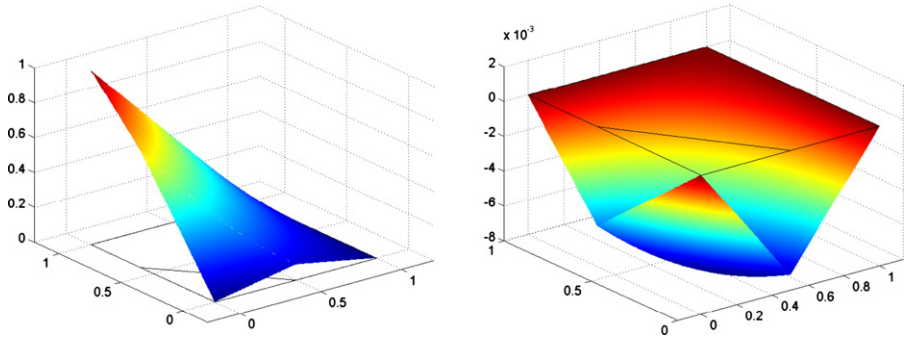

Fig. 6. The bilinear IFE basis functions $\hat{\mathbf{\Phi}}_3$ on the Type I reference element for planar elasticity interface problem: the left plot is for the first component of $\hat{\mathbf{\Phi}}_3$, and the right plot is for its second component with $\lambda^+ = 50$, $\lambda^- = 1$, $\mu^+ = 5$, $\mu^- = 2$, $\hat{D} = (0, 0.6)^t$, $\hat{E} = (0.5, 0)^t$.

$$m^{\mathrm{II}}_{V76} = -(\hat{d} + \hat{e})\lambda^+ - (\hat{d} - \hat{e})\mu^+, \qquad m^{\mathrm{II}}_{V86} = (\hat{d}^2 - \hat{e}^2)\omega^+ + \mu^+,$$
$$m^{\mathrm{II}}_{V77} = -(2 - \hat{d} - \hat{e})\lambda^- - (\hat{d} - \hat{e})\mu^-, \qquad m^{\mathrm{II}}_{V87} = (\hat{d}\hat{p} - \hat{e}\hat{q})\omega^-,$$
$$m^{\mathrm{II}}_{V78} = (\hat{d} + \hat{e})\lambda^+ - (\hat{d} - \hat{e})\mu^+, \qquad m^{\mathrm{II}}_{V88} = -(\hat{d}^2 - \hat{e}^2)\omega^+ + \mu^+.$$

Using $\mathbf{V} = \mathbf{V}_i = \mathbf{e}_i \in \mathbb{R}^8$, $1 \le i \le 8$ as the usual i-th basis vector, we can solve (3.14) for the vector $\mathbf{C} = \mathbf{C}_i$ and use them in (3.8), (3.9) or (3.10), (3.11) to form the i-th vector bilinear IFE nodal basis function $\hat{\mathbf{\Phi}}_i$ on either the Type I or Type II reference rectangle. Moreover, applying the affine mapping F between the reference element $\hat{T}$ and the actual element T, we obtain the bilinear IFE nodal basis functions on T as follows:

$$\mathbf{\Phi}_{i,T}(X) = \hat{\mathbf{\Phi}}_i(F^{-1}(X)) = \hat{\mathbf{\Phi}}_i(\hat{X}), \quad 1 \le i \le 8.$$

Finally, for each element $T \in \mathcal{T}_h$, we define the local linear IFE space $\mathbf{S}_h(T)$ as

$$\mathbf{S}_h(T) = \begin{cases} \mathrm{span}\{\mathbf{\Phi}_{i,T},\ 1 \le i \le 8\}, & \text{if } T \text{ is an interface rectangle,} \\ \mathrm{span}\{\mathbf{\Psi}_{i,T},\ 1 \le i \le 8\}, & \text{otherwise.} \end{cases} \tag{3.19}$$

Fig. 5 illustrates a standard vector bilinear nodal basis function on a non-interface element. As we can see, one component of this basis function is the same as the standard scalar bilinear nodal basis function, and the other one is simply the zero function. Figs. 6 and 7 provide illustrations for a vector-valued bilinear IFE basis function on the Type I and Type II interface rectangle, respectively. Note that one component of a vector bilinear IFE basis is similar to a scalar bilinear IFE nodal basis [33], but the other component cannot be completely zero in general due to interface jump conditions.

4. Properties of the linear and bilinear IFE functions

In this section, we show that linear and bilinear IFE functions for planar elasticity interface problems have some desirable properties usually expected for finite element functions.

4.1. Basic properties of the linear and bilinear IFE space

Assume $\mathcal{T}_h$ is a Cartesian triangular (resp. rectangular) mesh of Ω, and $(x_j, y_j)^t, j = 1, \ldots, N$ are the nodes of $\mathcal{T}_h$, where N denotes the total number of nodes. We define two linear (resp. bilinear) global nodal IFE basis functions $\mathbf{\Phi}_{2j-1}$ and $\mathbf{\Phi}_{2j}$

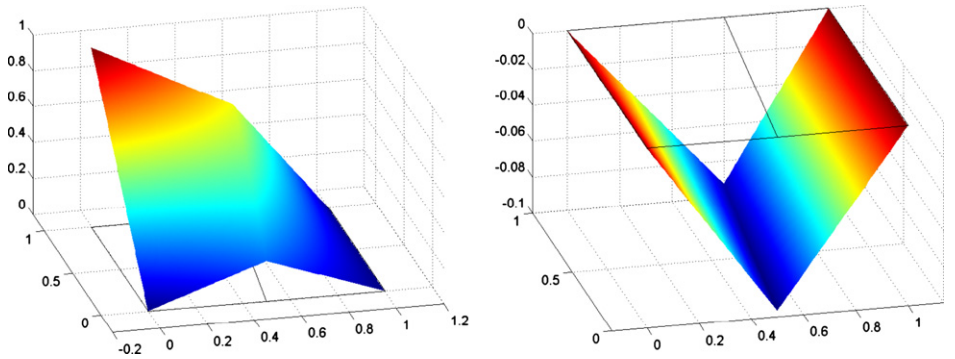

Fig. 7. The bilinear IFE basis functions $\hat{\Phi}_3$ on the Type II reference element for planar elasticity interface problem: the left plot is for the first component of $\hat{\Phi}_3$, and the right plot is for its second component with $\lambda^+ = 50$, $\lambda^- = 1$, $\mu^+ = 5$, $\mu^- = 2$, $\hat{D} = (0, 0.6)^t$, $\hat{E} = (0.5, 0)^t$.

associated to each node $(x_j, y_j)^t$ of $\mathcal{T}_h$, $j = 1, \ldots, N$, such that

$$\mathbf{\Phi}_{2i-1}(x_j, y_j) = \begin{cases} (1,0)^t, & \text{if } i = j, \\ (0,0)^t, & \text{if } i \neq j, \end{cases} \qquad \mathbf{\Phi}_{2i}(x_j, y_j) = \begin{cases} (0,1)^t, & \text{if } i = j, \\ (0,0)^t, & \text{if } i \neq j, \end{cases} \quad j = 1, \ldots, N,$$

and $\mathbf{\Phi}_k|_T \in \mathbf{S}_h(T)$, $k = 1, \ldots, 2N$, for every $T \in \mathcal{T}_h$. Finally, we define the linear (resp. bilinear) IFE space $\mathbf{S}_h(\Omega)$ over the whole domain Ω as the span of these global nodal IFE basis functions.

The following proposition shows that both linear and bilinear vector IFE functions are continuous within each element.

Proposition 4.1. *Let $\mathbf{S}_h(T)$ be the linear or bilinear vector-valued local IFE space on an interface element T. Then $\mathbf{S}_h(T) \subset \mathbf{C}(T)$.*

Proof. It suffices to show IFE functions are continuous across the line segment $\overline{DE}$. Assume $\mathbf{S}_h(T)$ is the linear IFE space, then every $\mathbf{\Phi} \in \mathbf{S}_h(T)$ is a vector-valued piece-wise linear function. Hence, the jump function $[\mathbf{\Phi}]_{\overline{DE}}$ is a vector-valued single variable linear polynomial. Therefore, $[\mathbf{\Phi}]_{\overline{DE}} = \mathbf{0}$ follows from $[\mathbf{\Phi}(D)] = [\mathbf{\Phi}(E)] = \mathbf{0}$ which implies that $\mathbf{\Phi}$ is continuous on T. Similar arguments can be used for the case in which $\mathbf{S}_h(T)$ is the bilinear IFE space. □

The properties given in the following proposition are easy to verify.

Proposition 4.2. *Let $\mathbf{S}_h(\Omega)$ be the linear (resp. bilinear) IFE space over the partition $\mathcal{T}_h$ of Ω, then*

- *$\mathbf{S}_h(\Omega)$ has the same dimension as the standard FE space formed by the usual vector-valued linear (resp. bilinear) polynomials on the same partition of Ω.*
- *Let Ω' denote the union of all interface elements, we have*

$$\mathbf{\Phi}|_{\Omega/\Omega'} \in \mathbf{H}^1(\Omega/\Omega'), \quad \forall\, \mathbf{\Phi} \in \mathbf{S}_h(\Omega). \tag{4.1}$$

Proposition 4.3. *Let $\mathbf{S}_h(T)$ be the linear vector-valued IFE space on T. Then every function $\mathbf{\Phi} \in \mathbf{S}_h(T)$ satisfies the traction jump condition on the actual interface $\Gamma \cap T$ weakly as follows:*

$$\int_{\Gamma \cap T} \left(\sigma(\mathbf{\Phi}^+) - \sigma(\mathbf{\Phi}^-)\right) \mathbf{n}_\Gamma \, ds = \mathbf{0}. \tag{4.2}$$

Proof. Let $T^* \subset T$ denote the region enclosed by $\Gamma \cap T$ and $\overline{DE}$. Note that for $s = +, -$, we have $\mathrm{div}\sigma(\mathbf{\Phi}^s) = \mathbf{0}$, since each $\mathbf{\Phi}^s$ is a linear vector-valued function. Applying the divergence theorem leads to the following identity:

$$\int_{\partial T^*} \left(\sigma(\mathbf{\Phi}^+) - \sigma(\mathbf{\Phi}^-)\right) \mathbf{n}_{T^*} ds = \int_{T^*} \left(\mathrm{div}\sigma(\mathbf{\Phi}^+) - \mathrm{div}\sigma(\mathbf{\Phi}^-)\right) dX = \mathbf{0}, \tag{4.3}$$

where $\mathbf{n}_{T^*}$ is the unit outer normal of T^*. Then, (4.2) follows from $\partial T^* = (\Gamma \cap T) \cup \overline{DE}$ and

$$\int_{\overline{DE}} \left(\sigma(\mathbf{\Phi}^+) - \sigma(\mathbf{\Phi}^-)\right) \mathbf{n}_{\overline{DE}} \, ds = \mathbf{0}. \quad \square$$

Remark 4.1. In general, if $\Gamma \cap T \neq \overline{DE}$, the weak traction continuity (4.2) is not true for functions $\mathbf{\Phi}$ in a bilinear local IFE space $\mathbf{S}_h(T)$ because $\mathrm{div}(\sigma(\mathbf{\Phi}))$ is generally nonzero unless we assume some extra conditions such as $[\lambda + \mu] = 0$.

Similar to the standard vector-valued linear (resp. bilinear) finite element spaces, the local basis functions of the linear (resp. bilinear) IFE space $\mathbf{S}_h(T)$ preserve the property of partition of unity.

Proposition 4.4. *Let $T \in \mathcal{T}_h$ be an interface element. Then*

$$\text{For bilinear IFE:} \quad \sum_{i=1}^{4} \mathbf{\Phi}_{i,T}(x,y) = \begin{pmatrix} 1 \\ 0 \end{pmatrix}, \qquad \sum_{i=5}^{8} \mathbf{\Phi}_{i,T}(x,y) = \begin{pmatrix} 0 \\ 1 \end{pmatrix}, \quad \forall\, (x,y)^t \in T. \tag{4.4}$$

$$\text{For linear IFE:} \quad \sum_{i=1}^{3} \mathbf{\Phi}_{i,T}(x,y) = \begin{pmatrix} 1 \\ 0 \end{pmatrix}, \qquad \sum_{i=4}^{6} \mathbf{\Phi}_{i,T}(x,y) = \begin{pmatrix} 0 \\ 1 \end{pmatrix}, \quad \forall\, (x,y)^t \in T. \tag{4.5}$$

Proof. For vector bilinear IFE local nodal basis functions $\hat{\mathbf{\Phi}}_i$ on a reference rectangle $\hat{T}$, by direct calculations, we can show

$$\sum_{i=1}^{4} \hat{\mathbf{\Phi}}_i(\hat{x},\hat{y}) = \begin{pmatrix} 1 \\ 0 \end{pmatrix}, \qquad \sum_{i=5}^{8} \hat{\mathbf{\Phi}}_i(\hat{x},\hat{y}) = \begin{pmatrix} 0 \\ 1 \end{pmatrix}, \quad \forall\, (\hat{x},\hat{y})^t \in \hat{T}. \tag{4.6}$$

Then, we use the affine mapping between the reference element $\hat{T}$ and the actual element T to obtain (4.4). Similar arguments can be carried out for linear IFE basis functions. □

The following proposition shows that the vector IFE functions are consistent with the standard finite element functions.

Proposition 4.5. *Let $T \in \mathcal{T}_h$ be an interface element, and $\mathbf{\Phi}_{i,T} \in \mathbf{S}_h(T)$ is one of the vector linear (resp. bilinear) local nodal basis functions. Then the following results are true:*

- *If the elasticity parameters have no discontinuity, i.e., $\lambda^+ = \lambda^-$, $\mu^+ = \mu^-$, then $\mathbf{\Phi}_{i,T}$ becomes the standard vector-valued linear (resp. bilinear) nodal basis $\mathbf{\Psi}_{i,T}$.*
- *If $\min\{|T^+|, |T^-|\}$ shrinks to 0, then $\mathbf{\Phi}_{i,T}$ becomes the standard vector linear (resp. bilinear) nodal basis $\mathbf{\Psi}_{i,T}$. Here $|T^s|$, $s = +, -$ is the area of the polygon T^s.*

Proof. For the first property, if we let $\lambda^+ = \lambda^-$, $\mu^+ = \mu^-$ in (2.11) or (3.14), then we can easily see $M_C = M_V$. This leads to $\mathbf{C} = \mathbf{V}$ in these equations, and by the definition of $\hat{\mathbf{\Phi}}_i$, we obtain the first property.

For the second property, let us consider the linear IFE functions, similar arguments work for bilinear IFE functions. Without loss of generality, let us assume $|\hat{T}^+|$ shrinks to zero. Then, we should have $\hat{d} \to 1$ or $\hat{e} \to 0$. Applying one of these to the solution $\mathbf{C}$ determined by (2.11), we can see $c_3 = v_3$ and $c_6 = v_6$. Then, the second property follows from the fact that $\hat{\mathbf{\Phi}}_i$ becomes $\hat{\mathbf{\Phi}}_i^-$ defined in (2.8) when $|\hat{T}^+|$ shrinks to zero. □

4.2. Unisolvent property for the linear and bilinear IFE basis

It is important to know whether the IFE functions always (uniquely) exist for any given Lamé parameters configuration and any possible interface location. This leads to the unisolvent property of the IFE functions: an IFE function is uniquely determined by its nodal values. We note that IFE functions developed for the interface problem of the second order elliptic equation have the unisolvent property [20,29,32,33]. However, since the differential operator in the planar linear elasticity problem is more complicated, whether IFE functions developed for the elasticity interface problem have the unisolvent property or not is not a trivial matter. In fact, the following counter-example suggests that the linear IFE functions do not always have this property.

Example 4.1. According to the reduced form (2.7) for the linear vector IFE functions, the unisolvent property is determined by the matrix M_C in (2.11). Suppose $\lambda^+ = 20$, $\lambda^- = 1$, $\mu^+ = 10$, $\mu^- = 1$. Let $\hat{d} = \frac{1}{100}$, and

$$\hat{e} = \frac{99\left(7097029 + 99\sqrt{23225041} - \sqrt{6114649667486 + 784726866\sqrt{23225041}}\right)}{626752400}$$
$$\approx 0.6994773141109332.$$

In this configuration of the interface points and elasticity parameters, the determinant $\det(M_C) = 0$. Also note that $\operatorname{rank}(M_C) = 5$, but $\operatorname{rank}([M_C, M_V\mathbf{V}_1]) = 6$. Therefore the linear system (2.11) has no solution and this implies the vector linear local nodal IFE basis functions $\hat{\mathbf{\Phi}}_1$ cannot be constructed in this case.

Hence, an intriguing question is that under what conditions these IFE functions are guaranteed to exist. To answer this question, we first investigate the determinant of the coefficient matrices M_C ($=M_C^{\mathrm{I}}$ or M_C^{II} depends on the interface element type) for the bilinear IFE functions. For the linear elasticity problem, we recall that Lamé parameters can be represented in terms of the *modulus of elasticity* E and the *Poisson's ratio* ν in the following way:

$$\lambda = \frac{E\nu}{(1+\nu)(1-2\nu)}, \qquad \mu = \frac{E}{2(1+\nu)}, \qquad \lambda = \frac{2\nu}{1-2\nu}\mu. \tag{4.7}$$

In many applications these parameters are such that $\lambda > 0, \mu > 0$, and $E > 0, 0 < \nu < \frac{1}{2}$. If ν is very close to $\frac{1}{2}$, corresponding materials become nearly incompressible. Also note that $\nu \approx \frac{1}{3}$ for many materials [38]. Our goal is to identify proper ranges of these parameters such that the vector IFE functions can be constructed for solving elasticity interface problems whose parameters are within these ranges.

We start with bilinear IFE functions. For the Type I interface rectangle, note that the determinant of M_C^{I} defined in (3.15) can be written as

$$\det(M_C^{\mathrm{I}}) = P_1^{\mathrm{I}}\lambda^+\mu^+ + P_2^{\mathrm{I}}\lambda^-\mu^+ + P_3^{\mathrm{I}}\mu^+\mu^+ + P_4^{\mathrm{I}}\lambda^+\mu^- + P_5^{\mathrm{I}}\lambda^-\mu^- + P_6^{\mathrm{I}}\mu^+\mu^- + P_7^{\mathrm{I}}\mu^-\mu^-, \tag{4.8}$$

where

$$\begin{aligned}
P_1^{\mathrm{I}} &= \hat{d}^2\hat{e}^2(\hat{d}^2+\hat{e}^2-4\hat{d})(\hat{d}^2+\hat{e}^2-4\hat{e}),\\
P_2^{\mathrm{I}} &= 4\hat{d}\hat{e}(\hat{d}+\hat{d}\hat{e}^2+\hat{e}+\hat{d}^2\hat{e}-4\hat{d}\hat{e}) + 2(\hat{d}^3+\hat{e}^3-2\hat{d}^2\hat{e}^2)\\
&\quad + (2+\hat{d}\hat{e})(\hat{d}^3(1-\hat{d})+\hat{e}^3(1-\hat{e})) + \hat{d}\hat{e}(3\hat{d}^3-2\hat{d}^2\hat{e}^2+3\hat{e}^3),\\
P_3^{\mathrm{I}} &= 2\hat{d}^2\hat{e}^2(-2\hat{d}+\hat{d}^2-2\hat{e}+\hat{e}^2)^2,\\
P_4^{\mathrm{I}} &= P_2^{\mathrm{I}},\\
P_5^{\mathrm{I}} &= (2\hat{d}^2-4\hat{d}^2\hat{e}+2\hat{e}^2+\hat{d}^3\hat{e}+\hat{d}\hat{e}^3)(2\hat{d}^2-4\hat{d}\hat{e}^2+2\hat{e}^2+\hat{d}^3\hat{e}+\hat{d}\hat{e}^3),\\
P_6^{\mathrm{I}} &= 4\hat{d}\hat{e}(2\hat{d}-\hat{d}^2+2\hat{e}-\hat{e}^2)(2\hat{d}^2-2\hat{d}^2\hat{e}+\hat{d}^3\hat{e}+2\hat{e}^2-2\hat{d}\hat{e}^2+\hat{d}\hat{e}^3),\\
P_7^{\mathrm{I}} &= 2(2\hat{d}^2-2\hat{d}^2\hat{e}+\hat{d}^3\hat{e}+2\hat{e}^2-2\hat{d}\hat{e}^2+\hat{d}\hat{e}^3)^2.
\end{aligned}$$

Simple calculation shows that $P_i^{\mathrm{I}} > 0, i = 2, \ldots, 7$ with $0 < \hat{d}, \hat{e} \le 1$. The only term that might be negative is P_1^{I}, which can make the entire determinant in (4.8) equal zero for some values $\hat{d}, \hat{e}$. On the other hand, the determinant of M_C^{I} can be bounded below under assumptions in the following lemma.

Lemma 4.1. *Assume there exist positives $\nu_0, \nu_1 \in (0, 1/2)$ and $m > 1$ such that the Poisson's ratios ν^s, and the Lamé parameters $\lambda^s, s = +, -$ of two coupled elastic materials satisfy*

$$\nu_0 \le \nu^s \le \nu_1, \quad s = +, -, \quad \text{and} \quad \frac{1}{m} \le \frac{\lambda^-}{\lambda^+} \le m. \tag{4.9}$$

Then the determinant of M_C^{I} is bounded below as follows

$$\det(M_C^{\mathrm{I}}) \ge F^{\mathrm{I}}(\hat{d}, \hat{e}, k, l, m)\lambda^+\mu^+, \tag{4.10}$$

where $k = \frac{2\nu_0}{1-2\nu_0}$, $l = \frac{2\nu_1}{1-2\nu_1}$, and

$$F^{\mathrm{I}}(\hat{d}, \hat{e}, k, l, m) = P_1^{\mathrm{I}} + \frac{1}{m}P_2^{\mathrm{I}} + \frac{1}{l}P_3^{\mathrm{I}} + \frac{k}{lm}P_4^{\mathrm{I}} + \frac{k}{lm^2}P_5^{\mathrm{I}} + \frac{1}{lm}P_6^{\mathrm{I}} + \frac{k}{l^2m^2}P_7^{\mathrm{I}}.$$

Proof. Combining (4.7) with (4.9), we obtain the following inequalities

$$\lambda^- \ge \frac{1}{m}\lambda^+, \qquad \mu^+ \ge \frac{1}{l}\lambda^+, \qquad \mu^- \ge \frac{1}{lm}\lambda^+, \qquad \mu^- \ge \frac{k}{lm}\mu^+. \tag{4.11}$$

Note that $P_i^{\mathrm{I}} \ge 0, i = 2, \ldots, 7$, then we can obtain (4.10) from (4.8) and (4.11). □

For Type II reference interface rectangle, the determinant of the coefficient matrix M_C^{II} is given by

$$\det(M_C^{\mathrm{II}}) = P_1^{\mathrm{II}}\lambda^+\mu^+ + P_2^{\mathrm{II}}\lambda^-\mu^+ + P_3^{\mathrm{II}}\mu^+\mu^+ + P_4^{\mathrm{II}}\lambda^+\mu^- + P_5^{\mathrm{II}}\lambda^-\mu^- + P_6^{\mathrm{II}}\mu^+\mu^- + P_7^{\mathrm{II}}\mu^-\mu^-, \tag{4.12}$$

where

$$\begin{aligned}
P_1^{\mathrm{II}} &= (\hat{d}-4\hat{d}^2+\hat{d}^3-3\hat{e}+4\hat{d}\hat{e}-\hat{d}^2\hat{e}-\hat{d}\hat{e}^2+\hat{e}^3)(-3\hat{d}+\hat{d}^3+\hat{e}+4\hat{d}\hat{e}-\hat{d}^2\hat{e}-4\hat{e}^2-\hat{d}\hat{e}^2+\hat{e}^3),\\
P_2^{\mathrm{II}} &= -\hat{d}^6+2\hat{d}^5(1+\hat{e})+\hat{d}^4(6-6\hat{e}+\hat{e}^2)-4\hat{d}^3(3-\hat{e}^2+\hat{e}^3)+\hat{d}^2(7+12\hat{e}-12\hat{e}^2+4\hat{e}^3+\hat{e}^4)\\
&\quad +\hat{e}(2+7\hat{e}-12\hat{e}^2+6\hat{e}^3+2\hat{e}^4-\hat{e}^5)+2\hat{d}(1-9\hat{e}+6\hat{e}^2-3\hat{e}^4+\hat{e}^5),\\
P_3^{\mathrm{II}} &= 2(-\hat{d}-2\hat{d}^2+\hat{d}^3-\hat{e}+4\hat{d}\hat{e}-\hat{d}^2\hat{e}-2\hat{e}^2-\hat{d}\hat{e}^2+\hat{e}^3)^2,\\
P_4^{\mathrm{II}} &= P_2^{\mathrm{II}},\\
P_5^{\mathrm{II}} &= (2-3\hat{d}+2\hat{d}^2+\hat{d}^3+\hat{e}-\hat{d}^2\hat{e}-2\hat{e}^2-\hat{d}\hat{e}^2+\hat{e}^3)(2+\hat{d}-2\hat{d}^2+\hat{d}^3-3\hat{e}-\hat{d}^2\hat{e}+2\hat{e}^2-\hat{d}\hat{e}^2+\hat{e}^3),\\
P_6^{\mathrm{II}} &= 4(2-\hat{d}+\hat{d}^3-\hat{e}-\hat{d}^2\hat{e}-\hat{d}\hat{e}^2+\hat{e}^3)(\hat{d}+2\hat{d}^2-\hat{d}^3+\hat{e}-4\hat{d}\hat{e}+\hat{d}^2\hat{e}+2\hat{e}^2+\hat{d}\hat{e}^2-\hat{e}^3),\\
P_7^{\mathrm{II}} &= 2(2-\hat{d}+\hat{d}^3-\hat{e}-\hat{d}^2\hat{e}-\hat{d}\hat{e}^2+\hat{e}^3)^2.
\end{aligned}$$

It is not difficult to see $P_i^{\mathrm{II}} > 0$, $i = 2, 3, 4, 6, 7$, for all $0 < \hat{d}, \hat{e} < 1$. However, it is possible for P_1^{II} and P_5^{II} to have negative values. The following lemma gives an estimate for the determinant of M_C^{II}.

Lemma 4.2. *Assume there exist positives $\nu_0, \nu_1 \in (0, 1/2)$ and $m > 1$ such that the Poisson's ratios ν^s, and the Lamé parameters λ^s, $s = +, -$ of two coupled elastic materials satisfy*

$$\nu_0 \le \nu^s \le \nu_1, \quad s = +, -, \quad \text{and} \quad \frac{1}{m} \le \frac{\lambda^-}{\lambda^+} \le m. \tag{4.13}$$

Then the determinant of M_C^{II} can be bounded below as follows

$$\det(M_C^{\mathrm{II}}) \ge F_1^{\mathrm{II}}(\hat{d}, \hat{e}, k, l, m)\lambda^+\mu^+ + F_2^{\mathrm{II}}(\hat{d}, \hat{e}, k, l, m)\lambda^-\mu^-, \tag{4.14}$$

where $k = \frac{2\nu_0}{1-2\nu_0}$, $l = \frac{2\nu_1}{1-2\nu_1}$, and

$$F_1^{\mathrm{II}}(\hat{d}, \hat{e}, k, l, m) = P_1^{\mathrm{II}} + \frac{1}{2m}P_2^{\mathrm{II}} + \frac{1}{l}P_3^{\mathrm{II}} + \frac{k}{2lm}P_4^{\mathrm{II}} + \frac{1}{2lm}P_6^{\mathrm{II}},$$
$$F_2^{\mathrm{II}}(\hat{d}, \hat{e}, k, l, m) = \frac{k}{2lm}P_2^{\mathrm{II}} + \frac{1}{2m}P_4^{\mathrm{II}} + P_5^{\mathrm{II}} + \frac{1}{2lm}P_6^{\mathrm{II}} + \frac{1}{l}P_7^{\mathrm{II}}.$$

Proof. Combining (4.7) with (4.13) leads to

$$\lambda^+ \ge \frac{1}{m}\lambda^-, \qquad \mu^- \ge \frac{1}{l}\lambda^-, \qquad \mu^+ \ge \frac{1}{lm}\lambda^-, \qquad \mu^+ \ge \frac{k}{lm}\mu^-. \tag{4.15}$$

We can write (4.12) as follows:

$$\begin{aligned}\det(M_C^{\mathrm{II}}) = &\left(P_1^{\mathrm{II}}\lambda^+\mu^+ + \frac{1}{2}P_2^{\mathrm{II}}\lambda^-\mu^+ + P_3^{\mathrm{II}}\mu^+\mu^+ + \frac{1}{2}P_4^{\mathrm{II}}\lambda^+\mu^- + \frac{1}{2}P_6^{\mathrm{II}}\mu^+\mu^-\right)\\ &+ \left(\frac{1}{2}P_2^{\mathrm{II}}\lambda^-\mu^+ + \frac{1}{2}P_4^{\mathrm{II}}\lambda^+\mu^- + P_5^{\mathrm{II}}\lambda^-\mu^- + \frac{1}{2}P_6^{\mathrm{II}}\mu^+\mu^- + P_7^{\mathrm{II}}\mu^-\mu^-\right).\end{aligned} \tag{4.16}$$

Combine (4.11) with the first term on the right hand side of (4.16) and combine (4.15) with the second term on the right hand side of (4.16), then we obtain (4.14). □

Note that F^{I}, F_1^{II}, and F_2^{II} are monotonically increasing with respect to k (hence monotonically decreasing with respect to ν_0), and monotonically decreasing with respect to l (hence monotonically increasing with respect to ν_1) and m. Hence, to find for which parameter configurations the bilinear IFE functions exist, we can use results of Lemmas 4.1 and 4.2 to find the largest possible m^* and ν_1^* and smallest possible ν_0^*, such that

$$F^{\mathrm{I}*}(\hat{d}, \hat{e}) = F^{\mathrm{I}}(\hat{d}, \hat{e}, k^*, l^*, m^*) > 0, \quad \forall\, 0 < \hat{d}, \hat{e} \le 1, \tag{4.17}$$
$$F_i^{\mathrm{II}*}(\hat{d}, \hat{e}) = F_i^{\mathrm{II}}(\hat{d}, \hat{e}, k^*, l^*, m^*) > 0, \quad \forall\, 0 < \hat{d}, \hat{e} < 1,\ i = 1, 2, \tag{4.18}$$

where $k^* = \frac{2\nu_0^*}{1-2\nu_0^*}$, $l^* = \frac{2\nu_1^*}{1-2\nu_1^*}$. A brief procedure in seeking k^*, l^*, and m^* is described as follows.

1. Set a maximal elasticity jump ratio, for instance $m^* = 10$, to determine the Poisson's ratio range within this jump.
2. Start with the least possible Poisson's ratio $\nu_0^* = 0$ and look for the largest possible ν_1^*.
3. For a given value $\hat{\nu}_1^*$, we let $\hat{l}^* = \frac{2\hat{\nu}_1^*}{1-2\hat{\nu}_1^*}$. Functions

   $$F^{\mathrm{I}}(\hat{d}, \hat{e}, k^*, \hat{l}^*, m^*), \qquad F_1^{\mathrm{II}}(\hat{d}, \hat{e}, k^*, \hat{l}^*, m^*), \quad \text{and} \quad F_2^{\mathrm{II}}(\hat{d}, \hat{e}, k^*, \hat{l}^*, m^*)$$

   become polynomials of $\hat{d}$ and $\hat{e}$, hence we can use algebraic tools to find their minima over the square domain $0 < \hat{d}, \hat{e} \le (\text{or} <) 1$.
4. Adjust the value of $\hat{\nu}_1^*$ according to the minima and repeat Step 3 until we find ν_1^* associated with $\nu_0^* = 0$.
5. Enlarge ν_1^*, and find the corresponding ν_0^* as another possible Poisson's ratio range obeys our choice of m^*.

Table 1 provides several possible configurations of ν_0^*, ν_1^* and m^* found according to the procedure above that guarantee (4.17) and (4.18). We summarize the above discussion in the following theorem.

Theorem 4.6. *Assume there exist positives ν_0^*, ν_1^*, and m^* satisfying (4.17) and (4.18). Assume the Poisson's ratios ν^s and the Lamé parameters λ^s, $s = +, -$ of two coupled elastic materials are such that*

$$\nu_0^* \le \nu^s \le \nu_1^*, \quad s = +, -, \quad \text{and} \quad \frac{1}{m^*} \le \frac{\lambda^-}{\lambda^+} \le m^*. \tag{4.19}$$

Then the bilinear IFE basis functions (3.7) for elasticity interface problem (1.1) uniquely exists.

Table 1
List of possible ranges that guarantee the unisolvent property of bilinear IFE nodal basis functions.

m^*	Possible (ν_0^*, ν_1^*)	Alternative (ν_0^*, ν_1^*)
10	(0, 0.45)	(0.02, 0.47)
20	(0, 0.40)	(0.12, 0.41)
40	(0, 0.35)	(0.22, 0.36)
60	(0, 0.32)	(0.03, 0.33)
80	(0, 0.31)	(0.16, 0.32)
100	(0, 0.30)	(0.21, 0.31)

Using similar arguments we can derive the unisolvent properties of linear nodal IFE basis on Cartesian triangular mesh. Note that the determinant of coefficient matrix M_C defined in (2.12) is given by

$$\det(M_C) = P_1\lambda^+\mu^+ + P_2\lambda^-\mu^+ + P_3\mu^+\mu^+ + P_4\lambda^+\mu^- + P_5\lambda^-\mu^- + P_6\mu^+\mu^- + P_7\mu^-\mu^-, \tag{4.20}$$

where

$$\begin{aligned}
P_1 &= (1 - 2\hat{d} + \hat{d}^2 - 3\hat{e} + 4\hat{d}\hat{e} - \hat{d}^2\hat{e} + 2\hat{e}^2)(1 - 2\hat{d} + \hat{d}^2 - \hat{e} + \hat{d}^2\hat{e} + 2\hat{d}\hat{e}^2),\\
P_2 &= (1 - \hat{d})\hat{e}^2(2 - 5\hat{d} + 4\hat{d}^2 - \hat{d}^3 - 4\hat{e} + 6\hat{d}\hat{e} - 2\hat{d}^2\hat{e} + 2\hat{e}^2),\\
P_3 &= 2(1 - 2\hat{d} + \hat{d}^2 - 2\hat{e} + 2\hat{d}\hat{e} + \hat{e}^2 + \hat{d}\hat{e}^2)^2,\\
P_4 &= P_2,\\
P_5 &= (1 - \hat{d})^3\hat{e}^2(-1 + \hat{d} + 2\hat{e}),\\
P_6 &= 4(1 - \hat{d})\hat{e}^2(1 - 2\hat{d} + \hat{d}^2 - 2\hat{e} + 2\hat{d}\hat{e} + \hat{e}^2 + \hat{d}\hat{e}^2),\\
P_7 &= 2(1 - \hat{d})^2\hat{e}^4.
\end{aligned}$$

In this case, only P_1 and P_5 might be negative. The following lemma provides an estimate for the determinant of M_C whose proof is similar as Lemma 4.2.

Lemma 4.3. *Assume there exist positives $\nu_0, \nu_1 \in (0, 1/2)$ and $m > 1$ such that the Poisson's ratios ν^s, and the Lamé parameters λ^s, $s = +, -$ of two coupled elastic materials satisfy*

$$\nu_0 \le \nu^s \le \nu_1, \quad s = +, -, \quad \text{and} \quad \frac{1}{m} \le \frac{\lambda^-}{\lambda^+} \le m. \tag{4.21}$$

Then the determinant of M_C can be bounded below as follows

$$\det(M_C) \ge F_1(\hat{d}, \hat{e}, k, l, m)\lambda^+\mu^+ + F_2(\hat{d}, \hat{e}, k, l, m)\lambda^-\mu^-, \tag{4.22}$$

where $k = \frac{2\nu_0}{1-2\nu_0}$, $l = \frac{2\nu_1}{1-2\nu_1}$, and

$$\begin{aligned}
F_1(\hat{d}, \hat{e}, k, l, m) &= P_1 + \frac{1}{2m}P_2 + \frac{1}{l}P_3 + \frac{k}{2lm}P_4 + \frac{1}{2lm}P_6,\\
F_2(\hat{d}, \hat{e}, k, l, m) &= \frac{k}{2lm}P_2 + \frac{1}{2m}P_4 + P_5 + \frac{1}{2lm}P_6 + \frac{1}{l}P_7.
\end{aligned}$$

Similarly, we have

Theorem 4.7. *Assume there exist positives $\tilde{\nu}_0^*$, $\tilde{\nu}_1^*$, and $\tilde{m}^*$ satisfying the following inequalities,*

$$F_i^*(\hat{d}, \hat{e}) = F_i(\hat{d}, \hat{e}, \tilde{k}^*, \tilde{l}^*, \tilde{m}^*) > 0, \quad \forall\, 0 < \hat{d}, \hat{e} \le 1,\ i = 1, 2, \tag{4.23}$$

where $\tilde{k}^* = \frac{2\tilde{\nu}_0^*}{1-2\tilde{\nu}_0^*}$, $l = \frac{2\tilde{\nu}_1^*}{1-2\tilde{\nu}_1^*}$, and assume the Poisson's ratios ν^s and the Lamé parameters λ^s, $s = +, -$ of two coupled elastic materials are such that

$$\tilde{\nu}_0^* \le \nu^s \le \tilde{\nu}_1^*, \quad s = +, -, \quad \text{and} \quad \frac{1}{\tilde{m}^*} \le \frac{\lambda^-}{\lambda^+} \le \tilde{m}^*.$$

Then the linear IFE basis functions (2.7) for elasticity interface problem (1.1) uniquely exists.

Some possible configurations for $\tilde{\nu}_0^*$, $\tilde{\nu}_1^*$, $\tilde{m}^*$ to guarantee (4.23) are given in Table 2.

Remark 4.2. Tables 1 and 2 indicate that bilinear IFE functions, compared with linear IFE functions, are guaranteed to be applicable to problems whose elasticity material parameters are chosen from a larger range of values and are allowed to have a larger discontinuity.

Table 2
List of possible ranges that guarantee the unisolvent property of linear IFE nodal basis functions.

$\tilde{m}^*$	Possible $(\tilde{\nu}_0^*, \tilde{\nu}_1^*)$
10	(0, 0.09)
20	(0, 0.04)

Table 3
Error of linear IFE interpolation $I_h\mathbf{u}$ with $\lambda^+ = 5$, $\lambda^- = 1$, $\mu^+ = 10$, $\mu^- = 2$.

N	$\|I_hu_1 - u_1\|_{L^2}$	$\|I_hu_1 - u_1\|_{H^1}$	$\|I_hu_2 - u_2\|_{L^2}$	$\|I_hu_2 - u_2\|_{H^1}$
10	3.1827×10^{-2}	4.2808×10^{-1}	8.1948×10^{-2}	1.1546×10^{-0}
20	8.0435×10^{-3}	2.1610×10^{-1}	2.0934×10^{-2}	5.8912×10^{-1}
40	2.0167×10^{-3}	1.0831×10^{-2}	5.2624×10^{-3}	2.9607×10^{-1}
80	5.0461×10^{-4}	5.4195×10^{-2}	1.3174×10^{-3}	1.4822×10^{-1}
160	1.2619×10^{-4}	2.7104×10^{-2}	3.2947×10^{-4}	7.4136×10^{-2}
320	3.1550×10^{-5}	1.3553×10^{-2}	8.2374×10^{-5}	3.7071×10^{-2}
640	7.8879×10^{-6}	6.7767×10^{-3}	2.0594×10^{-5}	1.8536×10^{-2}

4.3. Approximation properties of linear and bilinear IFE spaces

In this section, we numerically investigate the approximation properties of the linear and bilinear IFE spaces $\mathbf{S}_h(\Omega)$.

Assume $\mathcal{T}_h$ is a Cartesian mesh, triangular or rectangular. For each continuous vector-valued function $\mathbf{u} = (u_1, u_2)^t$ on an element $T \in \mathcal{T}_h$, we define its local IFE interpolation by

$$I_{h,T}\mathbf{u} = \begin{cases} \sum_{i=1}^{N_T} u_1(A_i)\boldsymbol{\Phi}_{i,T} + \sum_{i=N_T+1}^{2N_T} u_2(A_{i-N_T})\boldsymbol{\Phi}_{i,T}, & \forall\, T \in \mathcal{T}_h^i, \\ \sum_{i=1}^{N_T} u_1(A_i)\boldsymbol{\Psi}_{i,T} + \sum_{i=N_T+1}^{2N_T} u_2(A_{i-N_T})\boldsymbol{\Psi}_{i,T}, & \forall\, T \in \mathcal{T}_h^n, \end{cases} \tag{4.24}$$

where A_i, $1 \le i \le N_T$ are the vertices of T and $N_T = 3$ or 4 depending on whether T is triangular or rectangular. Then, for every $\mathbf{u} \in \mathbf{C}(\Omega)$, we piece-wisely define its global IFE interpolation $I_h\mathbf{u}$ by

$$I_h\mathbf{u}|_T = I_{h,T}\mathbf{u}. \tag{4.25}$$

We now use numerical experiments to test the approximation capability of these IFE spaces. Let $\Omega = (-1, 1) \times (-1, 1)$ be a rectangular domain. The interface curve Γ is a circle with radius $r_0 = \pi/8$ that separates Ω into two sub-domains $\Omega^+ = \{(x, y)^t : x^2 + y^2 > r_0^2\}$ and $\Omega^- = \{(x, y)^t : x^2 + y^2 < r_0^2\}$. Consider the function $\mathbf{u}$ defined as

$$\mathbf{u}(x, y) = \begin{pmatrix} u_1(x, y) \\ u_2(x, y) \end{pmatrix} = \begin{cases} \begin{pmatrix} u_1^-(x, y) \\ u_2^-(x, y) \end{pmatrix} = \begin{pmatrix} \frac{1}{\lambda^-} r^{\alpha_1} \\ \frac{1}{\lambda^-} r^{\alpha_2} \end{pmatrix}, & \text{if } (x, y)^t \in \Omega^-, \\ \begin{pmatrix} u_1^+(x, y) \\ u_2^+(x, y) \end{pmatrix} = \begin{pmatrix} \frac{1}{\lambda^+} r^{\alpha_1} + \left(\frac{1}{\lambda^-} - \frac{1}{\lambda^+}\right) r_0^{\alpha_1} \\ \frac{1}{\lambda^+} r^{\alpha_2} + \left(\frac{1}{\lambda^-} - \frac{1}{\lambda^+}\right) r_0^{\alpha_2} \end{pmatrix}, & \text{if } (x, y)^t \in \Omega^+, \end{cases} \tag{4.26}$$

where $\alpha_1 = 5$, $\alpha_2 = 7$, and $r = \sqrt{x^2 + y^2}$. The values of Lamé parameters are given as follows

$$\lambda = \begin{cases} \lambda^- = 1, & \text{in } \Omega^-, \\ \lambda^+ = 5, & \text{in } \Omega^+, \end{cases} \qquad \mu = \begin{cases} \mu^- = 2, & \text{in } \Omega^-, \\ \mu^+ = 10, & \text{in } \Omega^+. \end{cases}$$

To simplify the notation, we let $I_hu_1 = (I_h\mathbf{u})_1$, and $I_hu_2 = (I_h\mathbf{u})_2$. The errors of I_hu_1 and I_hu_2 using linear and bilinear IFE functions in L^2 and semi-H^1 norms are listed in Tables 3 and 4, respectively, where $h = 2/N$ is the mesh size for a Cartesian mesh $\mathcal{T}_h$. These data indicate

$$\|I_hu_i - u_i\|_{L^2} \approx \frac{1}{4}\|I_Hu_i - u_i\|_{L^2}, \qquad |I_hu_i - u_i|_{H^1} \approx \frac{1}{2}|I_Hu_i - u_i|_{H^1}, \quad i = 1, 2,$$

with $h = H/2$. To be more precise, using linear regression the interpolation errors listed in these tables obey:

Table 4
Error of bilinear IFE interpolation $I_h\mathbf{u}$ with $\lambda^+ = 5$, $\lambda^- = 1$, $\mu^+ = 10$, $\mu^- = 2$.

N	$\|I_hu_1 - u_1\|_{L^2}$	$\|I_hu_1 - u_1\|_{H^1}$	$\|I_hu_2 - u_2\|_{L^2}$	$\|I_hu_2 - u_2\|_{H^1}$
10	2.8715×10^{-2}	3.4737×10^{-1}	7.0919×10^{-2}	8.5496×10^{-1}
20	7.2498×10^{-3}	1.7538×10^{-1}	1.8088×10^{-2}	4.3494×10^{-1}
40	1.8173×10^{-3}	8.7916×10^{-2}	4.5452×10^{-3}	2.1844×10^{-1}
80	4.5468×10^{-4}	4.3992×10^{-2}	1.1378×10^{-3}	1.0934×10^{-1}
160	1.1370×10^{-4}	2.2002×10^{-2}	2.8453×10^{-4}	5.4685×10^{-2}
320	2.8428×10^{-5}	1.1002×10^{-2}	7.1138×10^{-5}	2.7345×10^{-2}
640	7.1072×10^{-6}	5.5009×10^{-3}	1.7785×10^{-5}	1.3673×10^{-2}

- Linear IFE Space:

$$\|I_hu_1 - u_1\|_{L^2} \approx 0.7970h^{1.9972}, \qquad |I_hu_1 - u_1|_{H^1} \approx 2.1437h^{0.9976},$$
$$\|I_hu_2 - u_2\|_{L^2} \approx 2.0565h^{1.9947}, \qquad |I_hu_2 - u_2|_{H^1} \approx 5.7939h^{0.9950}.$$

- Bilinear IFE Space:

$$\|I_hu_1 - u_1\|_{L^2} \approx 0.7189h^{1.9974}, \qquad |I_hu_1 - u_1|_{H^1} \approx 1.7394h^{0.9975},$$
$$\|I_hu_2 - u_2\|_{L^2} \approx 1.7792h^{1.9951}, \qquad |I_hu_2 - u_2|_{H^1} \approx 4.2877h^{0.9957}.$$

Therefore, we observe that interpolant $I_h\mathbf{u}$ produced with either linear or bilinear IFE functions converge to $\mathbf{u}$ with optimal rates in both L^2 norm and semi-H^1 norm.

5. An IFE Galerkin method for elasticity interface problem

In this section, we solve the planar elasticity interface problem (1.1)–(1.4) on Cartesian meshes using IFE functions developed in Section 3.

Assume that $\mathbf{u} \in \mathbf{H}^2(\Omega^s)$, $s = +, -$, satisfy (1.1) through (1.4). Multiply Eq. (1.1) by $\mathbf{v} \in \mathbf{H}_0^1(\Omega)$ and integrate over Ω^s, $s = +, -$:

$$-\int_{\Omega^s} \operatorname{div}\sigma(\mathbf{u}) \cdot \mathbf{v}\mathrm{d}X = \int_{\Omega^s} \mathbf{f} \cdot \mathbf{v}\mathrm{d}X. \tag{5.1}$$

Integration by parts using Green's formula leads to:

$$\int_{\Omega^s} \left(2\mu^s \epsilon(\mathbf{u}) : \epsilon(\mathbf{v}) + \lambda^s \operatorname{div}(\mathbf{u}) \operatorname{div}(\mathbf{v})\right) \mathrm{d}X - \int_{\Gamma} \sigma(\mathbf{u})\mathbf{n} \cdot \mathbf{v}\mathrm{d}s = \int_{\Omega^s} \mathbf{f} \cdot \mathbf{v}\mathrm{d}X, \tag{5.2}$$

where the inner product of two matrices $A = (A_{ij})$ and $B = (B_{ij})$ is defined by

$$A : B \triangleq \sum_{i=1}^{2}\sum_{j=1}^{2} A_{ij}B_{ij}.$$

Summing (5.2) over s, we obtain the following weak formulation for the linear elasticity interface problem: find $\mathbf{u} \in \mathbf{H}^1(\Omega)$ such that $\mathbf{u} = \mathbf{g}$ on $\partial\Omega$, and

$$a(\mathbf{u}, \mathbf{v}) = F(\mathbf{v}), \quad \forall \mathbf{v} \in \mathbf{H}_0^1(\Omega), \tag{5.3}$$

where

$$a(\mathbf{u}, \mathbf{v}) \triangleq \sum_{s=+,-} \int_{\Omega^s} \left(2\mu^s \epsilon(\mathbf{u}) : \epsilon(\mathbf{v}) + \lambda^s \operatorname{div}(\mathbf{u}) \operatorname{div}(\mathbf{v})\right) \mathrm{d}X, \quad \text{and} \quad F(\mathbf{v}) \triangleq \int_{\Omega} \mathbf{f} \cdot \mathbf{v}\,\mathrm{d}X. \tag{5.4}$$

This weak form leads to the following IFE method for the planar elasticity interface problem: find $\mathbf{u}_h = (u_{1h}, u_{2h})^t \in \mathbf{S}_h(\Omega)$ such that $\mathbf{u}_h = I_h\mathbf{g}$ on $\partial\Omega$, and

$$a_h(\mathbf{u}_h, \mathbf{v}_h) = F(\mathbf{v}_h), \quad \forall \mathbf{v}_h \in \mathbf{S}_{h,0}(\Omega), \tag{5.5}$$

where $\mathbf{S}_{h,0}(\Omega) = \{\mathbf{v} \in \mathbf{S}_h(\Omega), \mathbf{v}|_{\partial\Omega} = \mathbf{0}\}$, and

$$a_h(\mathbf{u}_h, \mathbf{v}_h) = \sum_{T \in \mathcal{T}_h} \int_T (2\mu\, \epsilon(\mathbf{u}_h) : \epsilon(\mathbf{v}_h) + \lambda \operatorname{div}(\mathbf{u}_h) \operatorname{div}(\mathbf{v}_h))\, \mathrm{d}X. \tag{5.6}$$

Numerical experiments are carried out using linear and bilinear IFE functions for the planar elasticity interface problem whose exact solution is given by (4.26). IFE solution errors in L^2 and semi-H^1 norms are computed by numerical quadratures

Table 5
Error of linear IFE solution $\mathbf{u}_h$ under triangular mesh with $\lambda^+ = 5, \lambda^- = 1, \mu^+ = 10, \mu^- = 2$.

N	$\|u_{1h} - u_1\|_{L^\infty}$	$\|u_{1h} - u_1\|_{L^2}$	$\|u_{1h} - u_1\|_{H^1}$	$\|u_{2h} - u_2\|_{L^\infty}$	$\|u_{2h} - u_2\|_{L^2}$	$\|u_{2h} - u_2\|_{H^1}$
10	1.3605×10^{-2}	3.8648×10^{-2}	4.3228×10^{-1}	1.7055×10^{-2}	7.7923×10^{-2}	1.1527×10^{-0}
20	3.7928×10^{-3}	9.8965×10^{-3}	2.1673×10^{-1}	4.7862×10^{-3}	1.9845×10^{-2}	5.8886×10^{-1}
40	9.6382×10^{-4}	2.4912×10^{-3}	1.0841×10^{-1}	1.2143×10^{-3}	4.9837×10^{-3}	2.9604×10^{-1}
80	2.4336×10^{-4}	6.2445×10^{-4}	5.4218×10^{-2}	3.3064×10^{-4}	1.2474×10^{-3}	1.4823×10^{-1}
160	7.4912×10^{-5}	1.5637×10^{-4}	2.7119×10^{-2}	1.2428×10^{-4}	3.1211×10^{-4}	7.4141×10^{-2}
320	4.6934×10^{-5}	3.9203×10^{-5}	1.3569×10^{-2}	5.2768×10^{-5}	7.8203×10^{-5}	3.7076×10^{-2}
640	2.2130×10^{-5}	9.8916×10^{-6}	6.7915×10^{-3}	2.5996×10^{-5}	1.9716×10^{-5}	1.8542×10^{-2}

Table 6
Error of bilinear IFE solution $\mathbf{u}_h$ under rectangular mesh with $\lambda^+ = 5, \lambda^- = 1, \mu^+ = 10, \mu^- = 2$.

N	$\|u_{1h} - u_1\|_{L^\infty}$	$\|u_{1h} - u_1\|_{L^2}$	$\|u_{1h} - u_1\|_{H^1}$	$\|u_{2h} - u_2\|_{L^\infty}$	$\|u_{2h} - u_2\|_{L^2}$	$\|u_{2h} - u_2\|_{H^1}$
10	1.3848×10^{-2}	3.3762×10^{-2}	3.5027×10^{-1}	1.8822×10^{-2}	8.1391×10^{-2}	8.5320×10^{-1}
20	3.3817×10^{-3}	8.5427×10^{-3}	1.7582×10^{-1}	4.7767×10^{-3}	2.0761×10^{-2}	4.3472×10^{-1}
40	8.4898×10^{-4}	2.1455×10^{-3}	8.7983×10^{-2}	1.2382×10^{-3}	5.2187×10^{-3}	2.1841×10^{-1}
80	2.1339×10^{-4}	5.3702×10^{-4}	4.4014×10^{-2}	3.2424×10^{-4}	1.3064×10^{-3}	1.0933×10^{-1}
160	8.5854×10^{-5}	1.3422×10^{-4}	2.2019×10^{-2}	9.3132×10^{-5}	3.2664×10^{-4}	5.5399×10^{-2}
320	4.6492×10^{-5}	3.3599×10^{-5}	1.1016×10^{-2}	3.4060×10^{-5}	8.1695×10^{-5}	2.7347×10^{-2}
640	2.2967×10^{-5}	8.4670×10^{-6}	5.5137×10^{-3}	1.4282×10^{-5}	2.0436×10^{-5}	1.3675×10^{-2}

with sufficient quadrature nodes over each element. IFE solution errors in the L^∞ norm are computed approximately as follows:

$$\|u_h - u\|_{L^\infty} = \max_{T \in \mathcal{T}_h} \left(\max_{\widetilde{T} \subset T} \left(\max_{(x,y) \in \widetilde{T}} |u_h(x,y) - u(x,y)| \right) \right), \tag{5.7}$$

where $\widetilde{T} = \{A_i : A_i \text{ are the vertices of the element } T\}$. Both moderate jump and large jump in Lamé parameters are experimented, and corresponding data are listed in Tables 5–8, respectively. Applying linear regression to the data in these tables yields the following estimates:

- Moderate jump: $\lambda^+ = 5, \lambda^- = 1, \mu^+ = 10, \mu^- = 2$,
  - Linear IFE solutions:

$$\|u_{1h} - u_1\|_{L^\infty} \approx 0.1241h^{1.5768}, \quad \|u_{1h} - u_1\|_{L^2} \approx 0.9631h^{1.9910}, \quad |u_{1h} - u_1|_{H^1} \approx 2.1601h^{0.9989},$$
$$\|u_{2h} - u_2\|_{L^\infty} \approx 0.1647h^{1.5846}, \quad \|u_{2h} - u_2\|_{L^2} \approx 1.9440h^{1.9935}, \quad |u_{2h} - u_2|_{H^1} \approx 5.7844h^{0.9947}.$$

  - Bilinear IFE solutions:

$$\|u_{1h} - u_1\|_{L^\infty} \approx 0.1092h^{1.5494}, \quad \|u_{1h} - u_1\|_{L^2} \approx 0.8420h^{1.9951}, \quad |u_{1h} - u_1|_{H^1} \approx 1.7503h^{0.9985},$$
$$\|u_{2h} - u_2\|_{L^\infty} \approx 0.2574h^{1.7532}, \quad \|u_{2h} - u_2\|_{L^2} \approx 2.0411h^{1.9948}, \quad |u_{2h} - u_2|_{H^1} \approx 4.2771h^{0.9946}.$$

- Large jump: $\lambda^+ = 1, \lambda^- = 100, \mu^+ = 2, \mu^- = 200$,
  - Linear IFE solutions:

$$\|u_{1h} - u_1\|_{L^\infty} \approx 1.6993h^{1.9725}, \quad \|u_{1h} - u_1\|_{L^2} \approx 4.8172h^{1.9940}, \quad |u_{1h} - u_1|_{H^1} \approx 10.795h^{0.9995},$$
$$\|u_{2h} - u_2\|_{L^\infty} \approx 1.9203h^{1.9337}, \quad \|u_{2h} - u_2\|_{L^2} \approx 9.7723h^{1.9957}, \quad |u_{2h} - u_2|_{H^1} \approx 5.7844h^{0.9947}.$$

  - Bilinear IFE solutions:

$$\|u_{1h} - u_1\|_{L^\infty} \approx 1.4018h^{1.9524}, \quad \|u_{1h} - u_1\|_{L^2} \approx 4.1549h^{1.9968}, \quad |u_{1h} - u_1|_{H^1} \approx 8.7436h^{0.9991},$$
$$\|u_{2h} - u_2\|_{L^\infty} \approx 1.7514h^{1.9328}, \quad \|u_{2h} - u_2\|_{L^2} \approx 10.170h^{1.9949}, \quad |u_{2h} - u_2|_{H^1} \approx 28.927h^{0.9947}.$$

These data demonstrate that both the linear and bilinear IFE solutions for the planar elasticity interface problem can converge at the optimal convergence rates in both L^2 and semi-H^1 norms. However, these data also indicate that, these IFE methods do not always converge optimally in the L^∞ norm. While these methods seem to converge optimally for the example with a large jump, they converge to the exact solution with a sub-optimal order in L^∞ norm for the example with a moderate jump. We note that similarly behavior is also observed for the IFE methods for the elliptic interface problems [32,33].

6. Conclusion

In this paper, we have discussed both the linear and bilinear IFE methods for planar elasticity interface problem with homogeneous jump conditions. These methods can use a Cartesian triangular/rectangular mesh instead of a traditional

Table 7
Error of linear IFE solution $\mathbf{u}_h$ under triangular mesh with $\lambda^+ = 1$, $\lambda^- = 100$, $\mu^+ = 2$, $\mu^- = 200$.

N	$\|u_{1h} - u_1\|_{L^\infty}$	$\|u_{1h} - u_1\|_{L^2}$	$\|u_{1h} - u_1\|_{H^1}$	$\|u_{2h} - u_2\|_{L^\infty}$	$\|u_{2h} - u_2\|_{L^2}$	$\|u_{2h} - u_2\|_{H^1}$
10	6.7359×10^{-2}	1.9191×10^{-1}	2.1576×10^{-0}	8.3069×10^{-2}	3.8959×10^{-1}	5.7636×10^{-0}
20	1.8644×10^{-2}	4.9111×10^{-2}	1.0818×10^{-0}	2.3699×10^{-2}	9.9175×10^{-2}	2.9442×10^{-0}
40	4.7635×10^{-3}	1.2365×10^{-2}	5.4108×10^{-1}	6.0280×10^{-3}	2.4903×10^{-2}	1.4801×10^{-0}
80	1.1976×10^{-3}	3.0970×10^{-3}	2.7056×10^{-1}	1.5185×10^{-3}	6.2325×10^{-3}	7.4109×10^{-1}
160	3.0049×10^{-4}	7.7476×10^{-4}	1.3528×10^{-1}	3.8005×10^{-4}	1.5585×10^{-3}	3.7067×10^{-1}
320	7.5104×10^{-5}	1.9364×10^{-4}	6.7642×10^{-2}	9.5094×10^{-5}	3.8965×10^{-4}	1.8535×10^{-1}
640	1.9192×10^{-5}	4.8369×10^{-5}	3.3821×10^{-2}	3.0496×10^{-5}	9.7408×10^{-5}	9.2678×10^{-2}

Table 8
Error of bilinear IFE solution $\mathbf{u}_h$ under rectangular mesh with $\lambda^+ = 1$, $\lambda^- = 100$, $\mu^+ = 2$, $\mu^- = 200$.

N	$\|u_{1h} - u_1\|_{L^\infty}$	$\|u_{1h} - u_1\|_{L^2}$	$\|u_{1h} - u_1\|_{H^1}$	$\|u_{2h} - u_2\|_{L^\infty}$	$\|u_{2h} - u_2\|_{L^2}$	$\|u_{2h} - u_2\|_{H^1}$
10	6.3499×10^{-2}	1.6581×10^{-1}	1.7473×10^{-0}	8.2680×10^{-2}	4.0535×10^{-1}	4.2655×10^{-0}
20	1.6043×10^{-2}	4.1991×10^{-2}	8.7728×10^{-1}	2.0796×10^{-2}	1.0344×10^{-1}	2.1735×10^{-0}
40	3.9988×10^{-3}	1.0535×10^{-2}	4.3900×10^{-1}	5.1989×10^{-3}	2.6001×10^{-2}	1.0920×10^{-0}
80	1.0028×10^{-3}	2.6363×10^{-3}	2.1954×10^{-1}	1.3236×10^{-3}	6.5093×10^{-3}	5.4667×10^{-1}
160	2.5086×10^{-4}	6.5926×10^{-4}	1.0978×10^{-1}	3.4695×10^{-4}	1.6279×10^{-3}	2.7342×10^{-1}
320	6.2895×10^{-5}	1.6478×10^{-4}	5.4890×10^{-2}	9.3999×10^{-5}	4.0700×10^{-4}	1.3672×10^{-1}
640	2.1016×10^{-5}	4.1188×10^{-5}	2.7446×10^{-2}	2.7678×10^{-5}	1.0175×10^{-4}	6.8361×10^{-2}

body-fitting mesh to handle problems with non-trivial interface geometries. Our numerical results indicate that the IFE interpolation errors and IFE solution errors have the optimal convergence rate in both L^2 and semi-H^1 norms, but IFE solutions may or may not converge optimally in L^∞ norm. The accuracies of these two IFE methods seem to be comparable, but the bilinear IFE method generally requires less time in assembling the involved algebraic system than the linear IFE method when their meshes have the same mesh size.

References

[1] A.P. Sutton, R.W. Balluffi, Interfaces in Crystalline Materials, Oxford Science Publications, 1995.
[2] H. Jou, P. Leo, J. Lowengrub, Microstructural evolution in inhomogeneous elastic media, J. Comput. Phys. 131 (1) (1997) 109–148.
[3] P. Leo, J. Lowengrub, Q. Nie, Microstructural evolution in orthotropic elastic media, J. Comput. Phys. 157 (1) (2000) 44–88.
[4] H. Gao, Y. Huang, F. Abraham, Continuum and atomistic studies of intersonic crack propagation, J. Mech. Phys. Solids 49 (9) (2001) 2113–2132.
[5] S. Brenner, L. Scott, The Mathematical Theorey of Finite Element Methods, Springer-Verlag, New York, 1994.
[6] P. Ciarlet, Mathematical Elasticity, Volume I: Three-Dimensional Elasticity, in: Studies in Mathematics and its Applications, vol. 20, North-Holland Publishing Co., Amsterdam, 1998.
[7] O.C. Zienkiewicz, R.L. Taylor, The Finte Element Method: Vol 2, Solid Mechanics, Butterworth-Heinemann, 2001.
[8] B. Cockburn, D. Schötzau, J. Wang, Discontinuous Galerkin methods for incompressible elastic materials, Comput. Methods Appl. Mech. Engrg. 195 (2006) 3184–3204.
[9] P. Hansbo, M.G. Larson, Discontinuous Galerkin and the Crouzeix–Raviart element: application to elasticity, M2AN Math. Model. Numer. Anal. 37 (1) (2003) 63–72.
[10] B. Rivière, S. Shaw, M. Wheeler, J. Whiteman, Discontinuous Galerkin finite element methods for linear elasticity and quasistatic linear viscoelasticity, Numer. Math. 95 (2) (2003) 347–376.
[11] T. Wihler, Locking-free adaptive discontinuous Galerkin FEM for linear elasticity problems, Math. Comp. 75 (255) (2006) 1087–1102.
[12] H. Xie, Z. Li, Z. Qiao, A finite element method for elasticity interface problems with locally modified triangulations, Int. J. Numer. Anal. Model. 8 (2) (2011) 189–200.
[13] I. Babuška, The finite element method for elliptic equations with discontinuous coefficients, Computing 5 (1970) 207–213.
[14] R. Becker, E. Burman, P. Hansbo, A Nitsche extended finite element method for incompressible elasticity with discontinuous modulus of elasticity, Comput. Methods Appl. Mech. Engrg. 198 (2009) 3352–3360.
[15] A. Hansbo, P. Hansbo, A finite element method for the simulation of strong and weak discontinuities in solid mechanics, Comput. Methods Appl. Mech. Engrg. 193 (2004) 3523–3540.
[16] X. Yang, B. Li, Z. Li, The immersed interface method for elasticity problems with interfaces, Dyn. Contin. Discrete Impuls. Syst. Ser. A Math. Anal. 10 (2003) 783–808.
[17] X. Yang, Immersed Interface Method for Elasticity Problems with interfaces, Ph.D. Thesis, North Carolina State University, 2004.
[18] Y. Gong, Z. Li, Immersed interface finite element methods for elasticity interface problems with non-homogeneous jump conditions, Numer. Math. Theory Methods Appl. 3 (1) (2010) 23–39.
[19] Z. Li, X. Yang, An immersed finite element method for elasticity equations with interfaces, in: Contemp. Math, in: Amer. Math. Soc., vol. 383, 2005, pp. 285–298.
[20] S. Adjerid, T. Lin, A p-th degree immersed finite element for boundary value problems with discontinuous coefficients, Appl. Numer. Math. 59 (6) (2009) 1303–1321.
[21] C. Attanayake, D. Senaratne, Convergence of an immersed finite element method for semilinear parabolic interface problems, Appl. Math. Sci. (Ruse) 5 (1–4) (2011) 135–147.
[22] B. Camp, T. Lin, Y. Lin, W. Sun, Quadratic immersed finite element spaces and their approximation capabilities, Adv. Comput. Math. 24 (1–4) (2006) 81–112.
[23] S. Chou, D. Kwak, K. Wee, Optimal convergence analysis of an immersed interface finite element method, Adv. Comput. Math. 33 (2) (2010) 149–168.
[24] R. Ewing, Z. Li, T. Lin, The immersed finite volume element methods for the elliptic interface problems, Math. Comput. Simul. 50 (1–4) (1999) 63–76.
[25] X. He, Bilinear immersed finite elements for interface problems, Ph.D. Thesis, Virginia Tech., 2009.
[26] X. He, T. Lin, Y. Lin, Approximation capability of a bilinear immersed finite element space, Numer. Methods Partial Differential Equations 24 (5) (2008) 1265–1300.

[27] X. He, T. Lin, Y. Lin, A bilinear immersed finite volume element method for the diffusion equation with discontinuous coefficient, Commun. Comput. Phys. 6 (1) (2009) 185–202.
[28] X. He, T. Lin, Y. Lin, Immersed finite element methods for elliptic interface problems with non-homogeneous jump conditions, Int. J. Numer. Anal. Model. 8 (2) (2011) 284–301.
[29] R. Kafafy, T. Lin, Y. Lin, J. Wang, Three-dimensional immersed finite element methods for electric field simulation in composite materials, Internat. J. Numer. Methods Engrg. 64 (7) (2005) 940–972.
[30] R. Kafafy, J. Wang, T. Lin, A hybrid-grid immersed-finite-element particle-in-cell simulation model of ion optics plasma dynamics, Dyn. Contin. Discrete Impuls. Syst. Ser. B Appl. Algorithms 12b (2005) 1–16.
[31] Z. Li, The immersed interface method using a finite element formulation, Appl. Numer. Math. 27 (3) (1998) 253–267.
[32] Z. Li, T. Lin, X. Wu, New Cartesian grid methods for interface problems using the finite element formulation, Numer. Math. 96 (1) (2003) 61–98.
[33] T. Lin, Y. Lin, R. Rogers, M. Ryan, A rectangular immersed finite element space for interface problems, Adv. Comput. Theory Pract. 7 (2001) 107–114.
[34] T. Lin, Y. Lin, W. Sun, Error estimation of a class of quadratic immersed finite element methods for elliptic interface problems, Discrete Contin. Dyn. Syst. Ser. B 7 (4) (2007) 807–823.
[35] S. Sauter, R. Warnke, Composite finite elements for elliptic boundary value problems with discontinuous coefficients, Computing 77 (1) (2006) 29–55.
[36] S. Vallaghé, T. Papadopoulo, A trilinear immersed finite element method for solving the electroencephalography forward problem, SIAM J. Sci. Comput. 32 (4) (2010) 2379–2394.
[37] Y. Gong, Immersed interface finite element methods for elliptic and elasticity interface problems, Ph.D. Thesis, North Carolina State University, 2007.
[38] D. Braess, Finite Elements Theory, Fast Solvers and Applications in Solid Mechanics, second ed., Cambridge University Press, 2001.